# An Approach to Simulate the Effects of Antenna Patterns on Polarimetric Variable Estimates

IGOR R. IVIĆ

*Cooperative Institute for Mesoscale Meteorological Studies, University of Oklahoma, and NOAA/OAR/National Severe Storms Laboratory, Norman, Oklahoma*

(Manuscript received 29 January 2017, in final form 11 April 2017)

ABSTRACT

One of the main challenges of using phased array radar for weather observations is the implementation of dual polarization with acceptable errors of polarimetric variable estimates. This is because the differences between the copolar antenna patterns at the horizontal and vertical polarizations, as well as cross-polar fields, can introduce unacceptable measurement biases, as the main beam is electronically steered away from the principal planes. Because the sufficient cross-polar isolation is difficult to achieve by the phased array antenna hardware and because the copolar as well as cross-polar patterns inevitably vary with each beam position, it is crucial to properly evaluate errors of estimates due to radiation patterns. Herein, a method that combines the measured or simulated radiation patterns and simulated time series is introduced. The method is suited for phased array and parabolic antennas, and it allows for evaluation of radiation-pattern-induced polarimetric variable biases and standard deviations specific to the antenna used to produce the patterns. The method can be used either as an alternative to a well-established approach using analytical derivations or as a tool for cross validation of the bias computations. For standard deviation evaluation in the presence of antenna cross-polar fields, the analytical approach becomes overly complex, which inexorably leads to the introduction of numerous approximations to obtain the results. These approximations inevitably compromise the accuracy of such computations. The method proposed herein avoids such approximations and therefore provides a valuable tool for accurate assessment of polarimetric measurement precision.

## 1. Introduction

The most recent advancement in operational weather radar technology is the introduction of dual polarization. It provides new information that improves the abilities of forecasters and algorithms to distinguish between different types of precipitation (e.g., rain, hail) and nonweather scatterers (e.g., insects, ground clutter), as well as more accurate quantitative precipitation estimation (QPE) (Zrnić and Ryzhkov 1999; Zrnić et al. 2001).

The most important polarimetric variables are the differential reflectivity $Z_{DR}$, the copolar correlation coefficient magnitude $|\rho_{hv}(0)|$ (herein referred to as correlation coefficient), and the differential phase $\phi_{DP}$ (Doviak and Zrnić 1993, section 8.5.2.3). The signals received by the radar are a measure of scatterer properties weighted by the horizontal (H) and vertical (V) copolar and cross-polar antenna patterns. The presence of cross-polar antenna patterns is due to a portion of the energy inserted into the H antenna port also being transmitted as the cross-polar V field, and vice versa. For a well-designed parabolic reflector, the main cross-polar lobes are positioned away from the main copolar lobe center, so the effects of cross-polar antenna patterns are negligible (e.g., WSR-88D; Zrnić et al. 2010). Nevertheless, slightly different H and V copolar beam shapes and/or pointing angles, and phase differences between copolar patterns, can induce notable biases in the estimates of polarimetric variables (Chandrasekar and Keeler 1993; Galletti and Zrnić 2011). For large phased array antennas, it is likely that H and V copolar pattern shapes will be well matched for boresight directions (i.e., the location of maximum antenna gain that ideally corresponds to the desired electronic beam steering direction) of interest because the array factor (i.e., the directional two-dimensional function, which weights the pattern shapes of individual radiators by means of controlling the relative phases and amplitudes of the radio waves emitted by the antenna elements in

*Corresponding author*: Igor Ivić, igor.ivic@noaa.gov

DOI: 10.1175/JTECH-D-17-0015.1

the array) is a highly peaked function relative to the smooth changes of the element patterns (Balanis 2005; section 6.10.1). But it is almost certain that the amplitude and phase of the copolar beams will differ and vary with beam direction (Lei et al. 2015; Balanis 2005). This effect induces bias in the estimates of polarimetric variables, herein referred to as copolar bias. For phased array antennas, the main lobe of cross-polar fields is coaxial with the main copolar lobe (as the beam is steered away from principal planes), so the effect of signals caused by cross-polar patterns cannot be neglected (Lei et al. 2015). The result is that cross-polar fields induce notable bias in the estimates of polarimetric variable estimates. In addition, because of a high level of component integration, coupling through hardware (e.g., the circuits behind the antenna backplane) is more likely than in radars using reflector antennas. Errors induced by these cross-coupling effects are herein referred to as cross-coupling bias. Because the next-generation of weather surveillance systems are envisioned to use the polarimetric phased array radar (PPAR) technology (Zrnić et al. 2007), the Second MPAR Symposium (http://www.ofcm.gov/groups/MPAR/meetings/symposium.htm, 17–19 November 2009) identified the polarimetric capability to be the most challenging technical issue for future multifunction phased array radar (MPAR) (Weadon et al. 2009).

The two typical modes of polarization implementation are the alternate (AHV) and simultaneous (SHV). In the AHV mode, the H and V ports of the antenna are alternately excited, whereas in the SHV mode the ports are excited simultaneously. The polarimetric measurements in the two modes are differently affected by the cross coupling. For the same antenna cross-polar isolation, the AHV is advantageous in that the bias of $Z_{DR}$ estimates is much smaller than in the SHV mode (Sachidananda and Zrnić 1985; Wang and Chandrasekar 2006). For example, if the cross-polar pattern has a peak coaxial with the copolar peak, and both patterns are of the same shape, then cross-polar suppression in excess of 50 dB is needed in the SHV mode to achieve the $Z_{DR}$ estimate bias of less than 0.1 dB (Zrnić et al. 2012; Ivić and Doviak 2016). The advantages of the SHV mode are as follows: 1) estimates of the polarimetric variables have significantly lower errors for large unambiguous range scans (Melnikov and Zrnić 2015), 2) the differential phase is unambiguous within a 360° interval, 3) the correlation coefficient and the differential phase are measured directly using returns from the same transmission (i.e., no need to combine second-order estimates from multiple transmissions), and 4) there are no compromises in the performance of the ground clutter filter (Zrnić et al. 2012). Despite these advantages, the fact that the polarimetric variable estimates are much less affected by the cross-polar antenna patterns in the AHV mode is a motivation to consider the application of this mode for higher-elevation scans (where unambiguous ranges are smaller).

Errors in polarimetric variable estimates induced by the mismatch between H and V copolar patterns and by the cross-polar fields have been analyzed extensively in the case of parabolic reflector antennas. Pointin et al. (1988) devised a method to estimate the $Z_{DR}$ bias due to only the mismatch of copolar patterns using the measurements of H and V illumination functions and the measured reflectivity factors. Chandrasekar and Keeler (1993), on the other hand, used measured powers of both copolar and cross-polar patterns of a reflector antenna to assess the $Z_{DR}$ bias. Because of the lack of phase information, they could assess only the upper bounds of errors via analytical derivations but were unable to quantify the actual biases induced by the measured antenna patterns. An analysis of the dual-polarized parabolic antenna performance characteristics is given in Bringi and Chandrasekar (2001, chapter 6). Therein, aspects of evaluating antenna polarimetric performance are presented in the case when spherical particles fill the radar beam with the emphasis on the AHV mode of operation. Using analytical derivations Zrnić et al. (2010) analyzed bias in $Z_{DR}$ estimates due to cross coupling through the radiation patterns for parabolic antennas in the SHV mode. The analysis showed that the bias in $Z_{DR}$ estimates is generally dependent on the intrinsic (i.e., true and not measured) signal parameters such as $Z_{DR}$, $|\rho_{hv}(0)|$, and $\phi_{DP}$ if scatterers are not spherical. Bias in $|\rho_{hv}(0)|$ caused by the antenna radiation patterns using analytical derivations and theoretical antenna patterns, for a reflector antenna, has been analyzed by Galletti and Zrnić (2011). They assessed the $|\rho_{hv}(0)|$ bias caused by unmatched H and V copolar radiation patterns as a function of slight differences in pointing angles and beamwidths, as well as cross-polar fields. Neither of these works, however, addresses the effects of radiation patterns on the polarimetric variables of phased array antennas.

On planar phased array antennas, the H and V copolar and cross-polar fields vary, as the beam is steered electronically. Therefore, the copolar and cross-coupling biases are different for each boresight direction (i.e., electronically steered beam direction). The copolar bias may be corrected using calibration, whereas the effects of cross-polar fields (i.e., cross-coupling bias) are more difficult to account for. The latter is because the cross-coupling biases change with the variation of the intrinsic signal parameters and therefore are not constant in range (Zrnić et al. 2010). Moreover, because of

the antenna design and manufacturing specifics, variations in copolar and cross-polar fields with beam direction are particular to each antenna. This compels us to search for ways of evaluating the polarimetric variable errors induced by the copolar and cross-polar fields that are pertinent to the phased array antenna of interest.

A well-established method to evaluate the polarimetric variables biases is via analytical computations (Chandrasekar and Keeler 1993; Bringi and Chandrasekar 2001; Wang and Chandrasekar 2006; Zrnić et al. 2010; Galletti and Zrnić 2011). For simplicity, this approach commonly introduces approximations such as discarding terms whose contribution is deemed insignificant, when computing the second-order estimates (used to compute the polarimetric variables). Also, in some cases, approximation via expansion into Taylor series is employed to obtain the expected values of polarimetric variables, which introduce errors that can go undetected if the results are not validated using an independent method.

While the main concern of the cited works is the cross-coupling bias, the cross coupling may also affect the standard deviation of estimates. Because of the complexity induced by the presence of cross-polar signals, an analysis of standard deviations using analytical derivations may introduce unacceptable errors and/or become intractable.

Consequently, the main objective herein is to introduce a method to simulate the effects of co- and cross-polar antenna patterns on polarimetric variable estimates. Because the computation of second-order estimates, using simulation, intrinsically accounts for all the terms and does not use Taylor series expansion (to obtain polarimetric variable ensemble averages), it can be used as a cross-validation tool or independently. The method is applicable to complex measured or simulated antenna patterns, specific to the phased array or parabolic antenna of interest. To devise such method, a previously developed model describing the echo voltages received by the parabolic reflector antenna is updated to accommodate the specifics of phased array antennas. Further, to provide a theoretical background for simulation, a standard concept where the backscattering matrix describes the backscattering properties of a single hydrometeor is modified whereby the properties of a collection of scatterers are described by the backscattering matrix.

The paper is structured as follows. In section 2, a theoretical model is introduced, while in section 3 generation of simulated time series is explained. Examples of bias and standard deviation computations are given in section 4. For bias computation, both the analytical and simulation bias results are presented for comparison. In the case of standard deviation, only the simulation results are presented due to the lack of proper analytical expressions caused by the complexity of their derivation. The main conclusions of the paper are summarized in section 5.

## 2. Theoretical model

Assuming a linear H, V polarization basis and no precipitation along the propagation path, the backscattering properties of a single canted hydrometeor can be described by its backscattering matrix $\mathbf{S}$, which relates the backscattered electric field vector $[\mathbf{E}]^b$ at the antenna to the one $[\mathbf{E}]^i$ incident on the scatterer [(8.39) in Doviak and Zrnić 1993],

$$[\mathbf{E}]^b = \begin{bmatrix} E_h \\ E_v \end{bmatrix}^b = \begin{bmatrix} s_{hh} & s_{hv} \\ s_{vh} & s_{vv} \end{bmatrix} \begin{bmatrix} E_h \\ E_v \end{bmatrix}^i \frac{\exp(-jkr)}{r}, \quad (1)$$

where $j = \sqrt{-1}$. Subscripts "h" and "v" denote the electric field's polarization, $k$ is the precipitation-free wavenumber, and $r$ is the distance from the radar to the scatterer.

Excitation of the antenna H port ideally generates purely horizontal (i.e., $E_h \equiv E_\phi$) electric fields, and excitation of the V port generates purely vertical (i.e., $E_v \equiv E_\theta$) electric fields. The $E_\theta$ and $E_\phi$ are electric field components in a spherical coordinate system with polar axis $z$ vertical, and $x$ is the direction broadside to the antenna (i.e., the antenna face is in the $y$–$z$ plane). Angles $\theta$ and $\phi$ are the zenith and azimuth directions to the scatterer (Fig. 1), respectively. In reality, excitation of the H or V ports always causes cross-polar fields to have an intensity determined by the radiation matrix $\mathbf{F}$ (Zrnić et al. 2010).

Further analysis is carried out assuming the following: 1) hydrometeors are oblate spheroids not canted (i.e., $s_{hv} = s_{vh} \approx 0$; Stapor and Pratt 1984), so no depolarization on propagation is present (Oguchi 1983; Sachidananda and Zrnić 1985); and 2) differential attenuation along the path of propagation can be, for most observations at 10-cm wavelengths, neglected but $\phi_{DP}$ (i.e., the phase difference between the H and V radiations caused by the difference in propagation delays) cannot. Generally, individual scatterers have canting angles that are not zero but in most cases the net mean canting angle (i.e., the angle between the incident vertically oriented electric field and the projection of the axis of symmetry on the plane of polarization) of raindrops contained in a sufficiently large volume of space is zero (Doviak et al. 2000; Ryzhkov et al. 2002; Ryzhkov and Zrnić 2007). In such a case, the summed cross-polarization returns

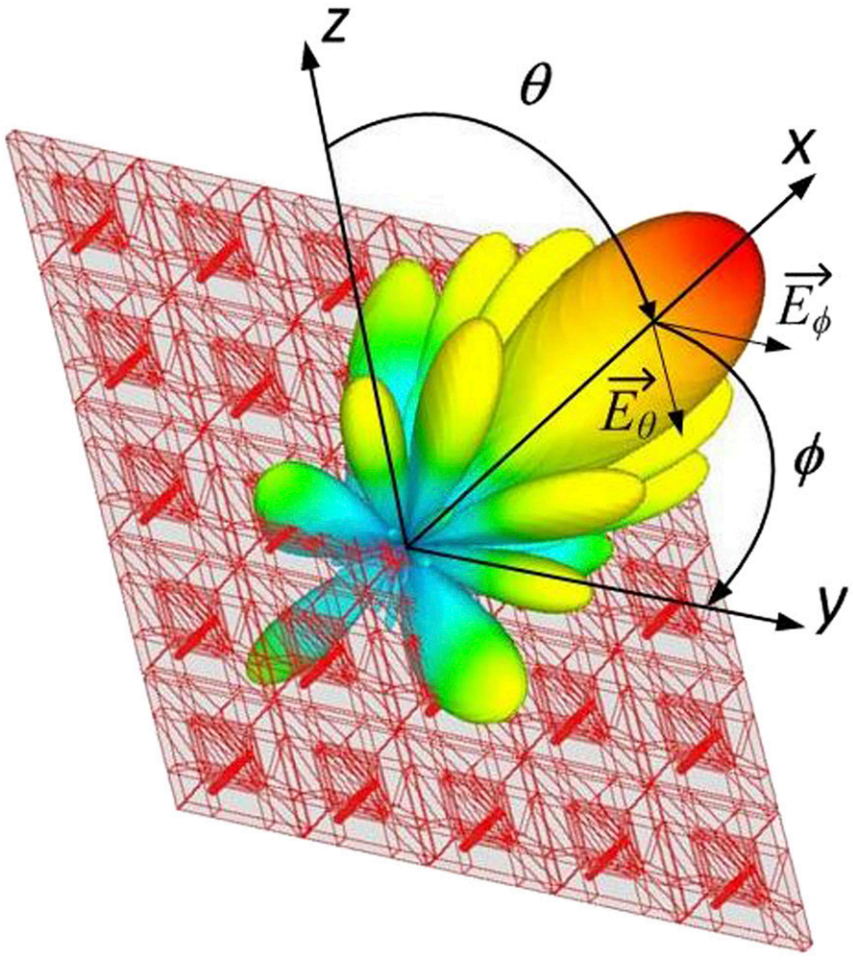


FIG. 1. A spherical coordinate system used to plot the radiation patterns.

from a large number of scatterers are close to zero [i.e., $\sum_n s_{vh}(n) = \sum_n s_{hv}(n) \approx 0$], and generalization can be introduced so that for each individual scatterer $s_{hv} = s_{vh} \approx 0$. This generalization provides the basis for the first assumption so that only depolarization incurred by the antenna cross-polar patterns is considered (i.e., $s_{hv} = s_{vh} \approx 0$). The errors introduced by both assumptions are bound by the extent of depolarization and differential attenuation induced by the scatterers, as these are not considered herein. The presented approach can be further expanded to include the presence of these effects and can be the topic for further research.

In either the SHV or AHV mode, echo voltages received after the $m$th transmission from the $n$th scatterer, located at range $\mathbf{r}_n$, are (Zrnić et al. 2010; Bringi and Chandrasekar 2001)

$$\begin{bmatrix} \delta V_h(\mathbf{r}_n, m) \\ \delta V_v(\mathbf{r}_n, m) \end{bmatrix} = C\mathbf{F}^T\mathbf{T}^T\mathbf{S}\mathbf{T}\mathbf{F}\mathbf{E}_P$$
$$= C \begin{bmatrix} F_{hh} & F_{vh} \\ F_{hv} & F_{vv} \end{bmatrix} \mathbf{T}^T \begin{bmatrix} s_{hh}(n) & 0 \\ 0 & s_{vv}(n) \end{bmatrix} \mathbf{T} \begin{bmatrix} F_{hh} & F_{hv} \\ F_{vh} & F_{vv} \end{bmatrix} \begin{bmatrix} A_h(m) \\ A_v(m)e^{j\beta} \end{bmatrix} e^{-j2kr_n(m)}, \quad (2)$$

where superscript "T" indicates the transposed matrix. Symbols $A_h(m)$ and $A_v(m)$ stand for the excitation amplitudes at the inputs of the H and V ports, respectively. Depending on the transmission mode they take values

$$\text{SHV: } A_h(m) = A_v(m) = 1$$
$$\text{AHV: } A_h(m) = \frac{1+(-1)^m}{2} \quad \text{and} \quad A_v(m) = \frac{1+(-1)^{m+1}}{2}. \tag{3}$$

In (2), $\mathbf{T}$ is the transmission matrix [(8.53) in Doviak and Zrnić 1993], which describes the effects of precipitation along the propagation path. Because only the differential phase effects are considered,

$$\mathbf{T} = \begin{bmatrix} \exp(-j\phi_{DP}/2) & 0 \\ 0 & 1 \end{bmatrix}. \tag{4}$$

Term $\mathbf{F}$ is the radiation matrix whose elements are one-way electric field patterns proportional to

$$\mathbf{F}_{lp}(\theta_0, \theta; \phi_0, \phi) = |\mathbf{F}_{lp}(\theta_0, \theta; \phi_0, \phi)| \exp[j\gamma_{lp}(\theta_0, \theta; \phi_0, \phi)], \tag{5}$$

where indices $l$ and $p$ can be either "h" or "v." Here $\mathbf{F}_{lp}(\theta_0, \theta; \phi_0, \phi)$ are complex pattern functions that depend on boresight direction $\theta_0$, $\phi_0$ in the case of phased array antennas but not in the case of parabolic reflectors. It is assumed that the measured or simulated complex electric field antenna patterns are produced in a form of a two-dimensional complex matrix in the Ludwig 2 coordinate system (Ludwig 1973) centered on the broadside of the antenna (the broadside is at $\theta = 90°$ and $\phi = 0°$) as shown in Fig. 1. Terms $\mathbf{F}_{hh}$ and $\mathbf{F}_{vv}$ are copolar electric field patterns. Term $\mathbf{F}_{hv}$ is the distribution of the radiated H cross-polar electric field if the V antenna port is excited, and vice versa for $\mathbf{F}_{vh}$. In (2), $\mathbf{E}_P$ is the isotropic transmitted electric field (i.e., not weighted by the transmit antenna patterns) so that the incident field on the $n$th scatterer is

$$[\mathbf{E}]^i \equiv \mathbf{TFE}_P = \begin{bmatrix} \exp(-j\phi_{DP}/2) & 0 \\ 0 & 1 \end{bmatrix} \begin{bmatrix} F_{hh}A_h(m) + F_{hv}A_v(m)e^{j\beta} \\ F_{vh}A_h(m) + F_{vv}A_v(m)e^{j\beta} \end{bmatrix} e^{-jkr_n(m)}. \tag{6}$$

The vector on the right side of (6) shows that the total H transmitted radiation, in the SHV mode, is a sum of the H copolar and V cross-polar radiations and vice versa for the total V radiation. If the net mean canting angle of hydrometeors along the propagation path is zero and attenuation can be neglected, then the matrix $\mathbf{T}$ in (6) describes the additional, propagation induced, phase difference (i.e., $\phi_{DP}/2$) between the H and V radiations that impinge on the $n$th scatterer. This phase is caused by the difference in propagation delays as the H and V radiations traverse space populated by the scatterers preceding the range $\mathbf{r}_n$ (where the $n$th scatterer is located). Because of the backscattered radiation propagation delay [described by $\mathbf{T}^T$ in (2)], the total propagation-induced phase difference between the H and V echoes from the $n$th scatterer that reaches the antenna is $\sim\phi_{DP}$ for hydrometeors at 10-cm wavelengths (Doviak and Zrnić 1993). Because of the cross-polar patterns, the signals received in the H and V channels are a combination of echoes returned in the two orthogonal planes [as described by $\mathbf{F}^T$ in (2)]. The result is that the bias of the H and V phase difference measured by the receiver is not constant and varies with the intrinsic signal parameters. For simplicity, the propagation-induced difference in phase between H and V is absorbed into the backscattering coefficient for horizontal polarization as $s'_{hh}(n) \equiv s_{hh}(n)\exp(-j\phi_{DP})$. The arguments of $F_{ll}$ in (2) are not explicitly shown, and $C$ is a scalar factor that contains dependence on range $r_0$ to resolution volume $V_6$ (i.e., volume encompassed by the radar beam and the range weighting function; Doviak and Zrnić 1993), attenuation, and system parameters. The phase difference between the H and V transmitter paths is denoted by $\beta$. For simplicity, the effects of the differences introduced by the H and V receiver paths (e.g., differential phase shifts between the H and V receivers) are neglected, as they have no bearing on the results reported herein.

The model in (2) assumes that the co- and cross-polar fields in H and V on transmit and receive are the same. This is true for parabolic antennas but generally not for phased array systems. To accommodate beamforming techniques and to maximize transmitted power efficiency, transmit/receive (T/R) elements allow application of different weights on transmit and receive on the single element level. Accordingly, the model in (2) is updated as

$$\begin{bmatrix} \delta V_h(\mathbf{r}_n, m) \\ \delta V_v(\mathbf{r}_n, m) \end{bmatrix} = C\mathbf{F}_r\mathbf{T}^T\mathbf{STF}_t\mathbf{E}_P$$
$$= C \begin{bmatrix} F_{rh}^{co} & F_{rh}^{x} \\ F_{rv}^{x} & F_{rv}^{co} \end{bmatrix} \begin{bmatrix} s'_{hh}(n) & 0 \\ 0 & s_{vv}(n) \end{bmatrix} \begin{bmatrix} F_{th}^{co} & F_{tv}^{x} \\ F_{th}^{x} & F_{tv}^{co} \end{bmatrix} \begin{bmatrix} A_h(m)e^{j\alpha_h(m)} \\ A_v(m)e^{j[\beta+\alpha_v(m)]} \end{bmatrix} e^{-j2kr_n(m)}, \tag{7}$$

where $F_{\rm th}^{\rm co}$ and $F_{\rm rh}^{\rm co}$ denote the copolar patterns in H on transmit and receive, respectively. Symbols $F_{\rm th}^{\rm x}$ and $F_{\rm rh}^{\rm x}$ denote the same but for cross-polar fields in H. Analogously, $F_{\rm tv}^{\rm co}$, $F_{\rm rv}^{\rm co}$, $F_{\rm tv}^{\rm x}$, and $F_{\rm rv}^{\rm x}$ denote the same but for co- and cross-polar patterns in V. Furthermore, to suppress the negative effects of cross coupling, a 180° pulse-to-pulse phase change of signals injected in either the horizontal or vertical ports of the transmission elements has been proposed by Zrnić et al. (2014) [with the detailed analysis given in Ivić and Doviak (2016)]. Hence, the model in (7) is updated to account for this phase coding method by adding the phases $\alpha_{\rm h}(m)$ and $\alpha_{\rm v}(m)$ on transmission. Note that if the phase coding is not applied, then $\alpha_{\rm h}(m)$ and $\alpha_{\rm v}(m)$ are set to zero. Carrying out the matrix multiplication, the H and V echo voltages are

$$\begin{aligned}\delta V_{\rm h}(\mathbf{r}_n,m) &= C\{[F_{\rm th}^{\rm co}F_{\rm rh}^{\rm co}s'_{\rm hh}(n)+F_{\rm th}^{\rm x}F_{\rm rh}^{\rm x}s_{\rm vv}(n)]A_{\rm h}(m)e^{j\alpha_{\rm h}(m)}\\ &\quad+[F_{\rm tv}^{\rm x}F_{\rm rh}^{\rm co}s'_{\rm hh}(n)+F_{\rm tv}^{\rm co}F_{\rm rh}^{\rm x}s_{\rm vv}(n)]A_{\rm v}(m)e^{j[\beta+\alpha_{\rm v}(m)]}\}e^{-j2kr_n(m)}.\\ \delta V_{\rm v}(\mathbf{r}_n,m) &= C\{[F_{\rm tv}^{\rm x}F_{\rm rv}^{\rm x}s'_{\rm hh}(n)+F_{\rm tv}^{\rm co}F_{\rm rv}^{\rm co}s_{\rm vv}(n)]A_{\rm v}(m)e^{j[\beta+\alpha_{\rm v}(m)]}\\ &\quad+[F_{\rm th}^{\rm co}F_{\rm rv}^{\rm x}s'_{\rm hh}(n)+F_{\rm th}^{\rm x}F_{\rm rv}^{\rm co}s_{\rm vv}(n)]A_{\rm h}(m)e^{j\alpha_{\rm h}(m)}\}e^{-j2kr_n(m)}.\end{aligned}\tag{8}$$

Then the returned echo voltages from the scatterers within the resolution volume $V_6$ at $\mathbf{r}_0$, after the $m$th transmission, in H and V are

$$V_l(\mathbf{r}_0,m)=\sum_n^{V_6}\delta V_l(\mathbf{r}_n,m)=V_l^{\rm co}(\mathbf{r}_0,m)+V_l^{\rm x}(\mathbf{r}_0,m),\tag{9}$$

where $l$ is h or v. In (9), $V_l^{\rm co}(\mathbf{r}_0, m)$ is the echo voltage from scatterers illuminated by the radiation described by $F_{tl}^{\rm co}$ whose returns are weighted by $F_{rl}^{\rm co}$ on reception. These are

$$\begin{aligned}V_{\rm h}^{\rm co}(\mathbf{r}_0,m)&=A_{\rm h}(m)C\sum_n^{V_6}F_{\rm th}^{\rm co}F_{\rm rh}^{\rm co}s'_{\rm hh}(n)e^{j\alpha_{\rm h}(m)}e^{-j2kr_n(m)}\\ V_{\rm v}^{\rm co}(\mathbf{r}_0,m)&=A_{\rm v}(m)C\sum_n^{V_6}F_{\rm tv}^{\rm co}F_{\rm rv}^{\rm co}s_{\rm vv}(n)e^{j[\beta+\alpha_{\rm v}(m)]}e^{-j2kr_n(m)}.\end{aligned}\tag{10}$$

The contributions to $V_l(\mathbf{r}_0, m)$ from scatterers illuminated by both the copolar and cross-polar radiation whose returns are weighted by the copolar and cross-polar patterns on reception are denoted by $V_l^{\rm x}(\mathbf{r}_0, m)$:

$$\begin{aligned}V_{\rm h}^{\rm x}(\mathbf{r}_0,m)&=C\sum_n^{V_6}\{F_{\rm th}^{\rm x}F_{\rm rh}^{\rm x}s_{\rm vv}(n)A_{\rm h}(m)e^{j\alpha_{\rm h}(m)}+[F_{\rm tv}^{\rm x}F_{\rm rh}^{\rm co}s'_{\rm hh}(n)+F_{\rm tv}^{\rm co}F_{\rm rh}^{\rm x}s_{\rm vv}(n)]A_{\rm v}(m)e^{j[\beta+\alpha_{\rm v}(m)]}\}e^{-j2kr_n(m)}.\\ V_{\rm v}^{\rm x}(\mathbf{r}_0,m)&=C\sum_n^{V_6}\{F_{\rm tv}^{\rm x}F_{\rm rv}^{\rm x}s'_{\rm hh}(n)A_{\rm v}(m)e^{j[\beta+\alpha_{\rm v}(m)]}+[F_{\rm th}^{\rm co}F_{\rm rv}^{\rm x}s'_{\rm hh}(n)+F_{\rm th}^{\rm x}F_{\rm rv}^{\rm co}s_{\rm vv}(n)]A_{\rm h}(m)e^{j\alpha_{\rm h}(m)}\}e^{-j2kr_n(m)}.\end{aligned}\tag{11}$$

The polarimetric variable estimates of interest are computed in the SHV mode as

$$\begin{aligned}\hat{Z}_{\rm DR}&=10\log_{10}\left(\frac{\hat{S}_{\rm h}}{\hat{S}_{\rm v}}\right)\\ |\hat{\rho}_{\rm hv}(0)|&=\frac{|\hat{R}_{\rm hv}(0)|}{\sqrt{\hat{S}_{\rm h}\hat{S}_{\rm v}}}\\ \hat{\phi}_{\rm DP}&=\arg[\hat{R}_{\rm hv}(0)],\end{aligned}\tag{12}$$

where $\hat{S}_{\rm h}$ and $\hat{S}_{\rm v}$ are the signal power estimates in the H and V channels, respectively, and $\hat{R}_{\rm hv}(0)$ is the cross-correlation estimate. These estimates are given as

$$\begin{aligned}\hat{S}_{\rm h}&=\frac{1}{M}\sum_{m=0}^{M-1}|V_{\rm h}(\mathbf{r}_0,m)|^2\\ \hat{S}_{\rm v}&=\frac{1}{M}\sum_{m=0}^{M-1}|V_{\rm v}(\mathbf{r}_0,m)|^2\\ \hat{R}_{\rm hv}(0)&=\frac{1}{M}\sum_{m=0}^{M-1}V_{\rm h}^{*}(\mathbf{r}_0,m)V_{\rm v}(\mathbf{r}_0,m)e^{j[\alpha_{\rm h}(m)-\alpha_{\rm v}(m)]},\end{aligned}\tag{13}$$

where $M$ stands for the number of samples in the dwell time (i.e., the time the radar spends scanning a particular location in space). Also, if phase coding is applied, then a correction must be applied to produce accurate $\hat{R}_{\rm hv}(0)$ [as shown in (13)]. The power estimates in H and V can be decomposed as

$$\hat{S}_l = \hat{S}_l^{\rm co} + \hat{S}_l^{\rm x}, \tag{14}$$

where

$$\hat{S}_l^{\rm co} = \frac{1}{M}\sum_{m=0}^{M-1}|V_l^{\rm co}(\mathbf{r}_0, m)|^2$$
$$\hat{S}_l^{\rm x} = \frac{1}{M}\sum_{m=0}^{M-1}[2{\rm Re}\{V_l^{\rm co}(\mathbf{r}_0, m)V_l^{x}(\mathbf{r}_0, m)\} + |V_l^{\rm x}(\mathbf{r}_0, m)|^2]. \tag{15}$$

Then, using the first-order Taylor expansion, in the case of $\hat{Z}_{\rm DR}$, the following is obtained:

$$\hat{Z}_{\rm DR} = 10\log_{10}\left(\frac{\hat{S}_{\rm h}^{\rm co} + \hat{S}_{\rm h}^{\rm x}}{\hat{S}_{\rm v}^{\rm co} + \hat{S}_{\rm v}^{\rm x}}\right) \approx 10\log_{10}\left(\frac{\hat{S}_{\rm h}^{\rm co}}{\hat{S}_{\rm v}^{\rm co}}\right) + \frac{10}{\ln(10)}\left(\frac{\hat{S}_{\rm h}^{\rm x}}{\hat{S}_{\rm h}^{\rm co}} - \frac{\hat{S}_{\rm v}^{\rm x}}{\hat{S}_{\rm v}^{\rm co}}\right), \tag{16}$$

where the first term in the sum is the contribution to $\hat{Z}_{\rm DR}$ from scatterers illuminated by radiation described by $F_{\rm th}^{\rm co}$, $F_{\rm tv}^{\rm co}$ whose returns are weighted by $F_{\rm rh}^{\rm co}$, $F_{\rm rv}^{\rm co}$ on reception. The second term is the contribution to $\hat{Z}_{\rm DR}$ from scatterers illuminated by both the copolar and cross-polar radiation whose returns are weighted by the copolar and cross-polar patterns on reception.

### a. *Errors of estimates*

If the antenna is pointed vertically (in light rain with no wind), then oblate raindrops appear "spherical" to the radar and $s_{\rm hh}(n) \approx s_{\rm vv}(n)$, which translates into $Z_{\rm DR} = 0\,{\rm dB}$, and $|\rho_{\rm hv}(0)| = 1$. In such cases, the analytical expressions for biases may be simplified because the biases are not functions of intrinsic hydrometer properties. For example, the first term in the (16) sum is

$$10\log_{10}\left(\frac{\hat{S}_{\rm h}^{\rm co}}{\hat{S}_{\rm v}^{\rm co}}\right) = 10\log_{10}\left(\frac{\int_\Omega F_{\rm th}^{\rm co}F_{\rm rh}^{\rm co}\,d\Omega}{\int_\Omega F_{\rm tv}^{\rm co}F_{\rm rv}^{\rm co}\,d\Omega}\right), \tag{17}$$

where $d\Omega \equiv \sin\theta d\theta d\phi$. If $F_{\rm th}^{\rm co} = F_{\rm rh}^{\rm co}$ and $F_{\rm tv}^{\rm co} = F_{\rm rv}^{\rm co}$, then (17) becomes the same result as obtained by Bringi and Chandrasekar [2001; (6.25)] and describes the $Z_{\rm DR}$ bias due to the copolar pattern mismatch (i.e., the copolar bias). The same approach can be taken to arrive at the expression for the second term in (16), which would describe the $Z_{\rm DR}$ bias due to the presence of cross-polar patterns (i.e., the cross-coupling bias) in the case of spherical particles. Accordingly, the expressions for $|\hat{\rho}_{\rm hv}(0)|$ and $\hat{\phi}_{\rm DP}$ may be obtained in this manner if scatterers are assumed spherical.

Because the cross-coupling biases in phased arrays are significant and depend on the intrinsic hydrometeor parameters, it is imperative to evaluate them in the general case when scatterers are not spherical. If scatterers are oblate, then $s_{\rm hh}(n) \neq s_{\rm vv}(n)$, which translates into $Z_{\rm DR} \neq 0\,{\rm dB}$, and $|\rho_{\rm hv}(0)| < 1$. In such cases, the biases are functions of intrinsic hydrometer properties and the derivation of analytical expressions for the copolar and cross-coupling biases becomes more complex. Assuming uniformly distributed oblate scattering particles with identical bulk properties (i.e., properties of a large number of scatterers)—so that $Z_{\rm DR}$, $|\rho_{\rm hv}(0)|$, and $\phi_{\rm DP}$ are the same within the H and V antenna beams—an approach using development into Taylor series [as in (16) and also presented in Zrnić et al. (2010)] can be used to derive the copolar and cross-coupling $Z_{\rm DR}$ biases by obtaining the expected values of the first and second terms in (16), respectively. Alternatively, the expansion in Taylor series can be avoided by computing the $Z_{\rm DR}$ bias directly [using (A10)]. A similar approach may be taken to arrive at the copolar and cross-coupling biases of $|\hat{\rho}_{\rm hv}(0)|$ and $\hat{\phi}_{\rm DP}$ (appendix A).

If the AHV mode is used, then the computations to produce the polarimetric variable estimates are more complex. These are as follows (Melnikov and Zrnić 2015):

$$\hat{Z}_{\rm DR} = 10\log_{10}\left(\frac{\hat{S}_{\rm h}}{\hat{S}_{\rm v}}\right)$$
$$|\hat{\rho}_{\rm hv}(0)| = \frac{|\hat{R}_a| + |\hat{R}_b|}{2(\hat{S}_{\rm h}\hat{S}_{\rm v})^{3/8}|\hat{R}_{\rm h}(2)\hat{R}_{\rm v}(2)|^{1/8}}$$
$$\hat{\phi}_{\rm DP} = \arg[\hat{R}_a\hat{R}_b^*]/2, \tag{18}$$

where

$$\hat{S}_{\rm h} = \frac{2}{M}\sum_{m=0}^{M/2-1}|V_{\rm h}(\mathbf{r}_0, 2m)|^2$$
$$\hat{S}_{\rm v} = \frac{2}{M}\sum_{m=0}^{M/2-1}|V_{\rm v}(\mathbf{r}_0, 2m+1)|^2$$
$$\hat{R}_a = \frac{2}{M}\sum_{m=0}^{M/2-1}V_{\rm h}^*(2m)V_{\rm v}(2m+1)$$
$$\hat{R}_b = \frac{1}{M/2-1}\sum_{m=0}^{M/2-2}V_{\rm h}(2m+2)V_{\rm v}^*(2m+1)$$
$$\hat{R}_{\rm h}(2) = \frac{2}{M}\sum_{m=0}^{M/2-1}V_{\rm h}^*(2m)V_{\rm h}(2m+2)$$
$$\hat{R}_{\rm v}(2) = \frac{2}{M}\sum_{m=0}^{M/2-1}V_{\rm v}^*(2m+1)V_{\rm v}(2m+3). \tag{19}$$

Analytical expressions for biases in the AHV mode are given in appendix B.

An alternative to using analytical derivation, for bias evaluation, are simulations. These simulations can also be used for a two-way verification of bias results (i.e., both simulation and analytical results should agree). If the standard deviation evaluation of the expressions in (12) and (18) is of interest, then the analytical derivations become excessively complex due to the presence of cross coupling. Consequently, this introduces a necessity for the introduction of multiple approximations to arrive at the solution. In turn, such approximations may compromise the accuracy of the final results. This makes simulations a viable alternative to analytical derivations for standard deviation computations (both in terms of implementation simplicity and accuracy). This is the motivation for devising a simulation method capable of evaluating errors in polarimetric variable estimates caused by the antenna radiation patterns. The theoretical background for such a simulation method is described next.

### b. Simulation approach

To devise the simulation, the approaches for generating weather-like time series described in Zrnić (1975) and Galati and Pavan (1995) are used. In Zrnić (1975), the basic process of generating single-polarization radar time series from Doppler spectra is outlined given the preset true values of Doppler moments. Galati and Pavan (1995) described an approach that uses the time series produced by Zrnic's method to generate the dual-polarization time series given the true values of polarimetric variables. Thus, the two methods provide an avenue for the generation of simulated weather-like time series that describe echoes from a large collection of scatterers contained in a volume of space illuminated by the radar beam. The obtained time series, however, do not account for the effects induced by the system imperfections that are of interest here (i.e., the existence of cross-polar radiation and the differences between the H and V antenna patterns). Consequently, the following is a description of an approach that combines these time series simulation methods with the antenna patterns to produce the weatherlike time series that account for the cross coupling and the differences between the H and V antenna patterns.

To provide the theoretical framework to use with the Zrnić (1975) and Galati and Pavan (1995) methods (which simulate returns from a large number of scatterers), the echo voltages from individual scatterers in $V_6$ at $\mathbf{r}_0$ are viewed as the sums of differential voltages caused by scatterers in subvolumes $dV_6$ (bound by the resolution of antenna patterns in azimuth and elevation) at $\mathbf{r}$. Thus, the differential voltage from scatterers in $dV_6$ is a sum of returns from a collection of particles described as

$$dV_l(\mathbf{r},m) = \sum_n \delta V_l(\mathbf{r}_n,m), \tag{20}$$

where $l$ is h or v. Because antenna patterns are practically constant over each $dV_6$, the substitution of (8) into (20) yields

$$\begin{aligned} dV_{\rm h}(\mathbf{r},m) = C\sum_n \{&[F_{\rm th}^{\rm co}F_{\rm rh}^{\rm co}s'_{\rm hh}(n) + F_{\rm th}^{\rm x}F_{\rm rh}^{\rm x}s_{\rm vv}(n)]A_{\rm h}(m)e^{j\alpha_{\rm h}(m)} \\ &+ [F_{\rm tv}^{\rm x}F_{\rm rh}^{\rm co}s'_{\rm hh}(n) + F_{\rm tv}^{\rm co}F_{\rm rh}^{\rm x}s_{\rm vv}(n)]A_{\rm v}(m)e^{j[\beta+\alpha_{\rm v}(m)]}\}e^{-j2kr_n(m)} \\ dV_{\rm v}(\mathbf{r},m) = C\sum_n \{&[F_{\rm tv}^{\rm x}F_{\rm rv}^{\rm x}s'_{\rm hh}(n) + F_{\rm tv}^{\rm co}F_{\rm rv}^{\rm co}s_{\rm vv}(n)]A_{\rm v}(m)e^{j[\beta+\alpha_{\rm v}(m)]} \\ &+ [F_{\rm th}^{\rm co}F_{\rm rv}^{\rm x}s'_{\rm hh}(n) + F_{\rm th}^{\rm x}F_{\rm rv}^{\rm co}s_{\rm vv}(n)]A_{\rm h}(m)e^{j\alpha_{\rm h}(m)}\}e^{-j2kr_n(m)}. \end{aligned} \tag{21}$$

Assuming scatterers of various equivalent volume diameters are uniformly distributed within $dV_6$, a subvolume scattering matrix $\mathbf{S}$, for each $dV_6$, can be defined as having elements

$$\begin{aligned} s'_{\rm hh}(m) &= C\sum_n s'_{\rm hh}(n)e^{-j2kr_n(m)} \\ s_{\rm vv}(m) &= C\sum_n s_{\rm vv}(n)e^{-j2kr_n(m)}, \end{aligned} \tag{22}$$

only on the main diagonal of $\mathbf{S}$. Elements of $\mathbf{S}$ account for the replacement of scatterers within $dV_6$ between subsequent transmissions, as well as the fact that scatterers have different relative ranges for every $m$. Also, wobbling and oscillations of scatterers within $dV_6$ produce a slight decorrelation between $s'_{\rm hh}(m)$ and $s_{\rm vv}(m)$, resulting in $|\rho_{\rm hv}(0)|$ values below one. Consequently, differential voltages have random real and imaginary parts that are zero mean and Gaussian distributed functions of $m$. Note that the dependence of $s'_{\rm hh}(m)$ and $s_{\rm vv}(m)$ on $m$ is clearly stated to differentiate these from the scattering matrix elements of a single scatterer. Thus, "$s$" and $\mathbf{S}$ henceforth will represent the subvolume scattering matrix elements. Now, the differential H and V voltages from $dV_6$ at $\mathbf{r}$ can be expressed as

$$dV_{\rm h}(\mathbf{r},m) = [F_{\rm th}^{\rm co}F_{\rm rh}^{\rm co}s'_{\rm hh}(m) + F_{\rm th}^{\rm x}F_{\rm rh}^{\rm x}s_{\rm vv}(m)]A_{\rm h}(m)e^{j\alpha_{\rm h}(m)} + [F_{\rm tv}^{\rm x}F_{\rm rh}^{\rm co}s'_{\rm hh}(m) + F_{\rm tv}^{\rm co}F_{\rm rh}^{\rm x}s_{\rm vv}(m)]A_{\rm v}(m)e^{j[\beta+\alpha_{\rm v}(m)]}$$
$$dV_{\rm v}(\mathbf{r},m) = [F_{\rm tv}^{\rm x}F_{\rm rv}^{\rm x}s'_{\rm hh}(m) + F_{\rm tv}^{\rm co}F_{\rm rv}^{\rm co}s_{\rm vv}(m)]A_{\rm v}(m)e^{j[\beta+\alpha_{\rm v}(m)]} + [F_{\rm th}^{\rm co}F_{\rm rv}^{\rm x}s'_{\rm hh}(m) + F_{\rm th}^{\rm x}F_{\rm rv}^{\rm co}s_{\rm vv}(m)]A_{\rm h}(m)e^{j\alpha_{\rm h}(m)}. \quad (23)$$

It is to be understood that although **r** does not explicitly appear on the right side of (23), it is implicit in the arguments of $s_{ll}(m)$. Also, $s_{ll}(m)$, $F_{ql}^{\rm co}$, and $F_{ql}^{\rm x}$ ($q$ is t or r and $l$ is h or v) depend on the angular arguments $\theta_0, \theta, \phi_0$, and $\phi$. The total received voltage for the $m$th sample is an integration over $\theta$ and $\phi$,

$$V_l(\mathbf{r}_0,m) = \int_\Omega dV_l(\mathbf{r},m)\,d\Omega + n_l(m), \quad (24)$$

where the subscript $l$ is h or v. In (24), integration along range is omitted, as it has no bearing on the results. The symbol $n_l(m)$ stands for voltage produced by white Gaussian noise and is added for completeness [unlike in (9)].

In the SHV mode, the signal power estimates $\hat{S}_{\rm h}$ and $\hat{S}_{\rm v}$ and $\hat{R}_{\rm hv}(0)$ are computed by following (13) as

$$\hat{S}_{\rm h} = \frac{1}{M}\sum_{m=0}^{M-1}\left|\int_\Omega dV_{\rm h}(\mathbf{r},m)\,d\Omega + n_{\rm h}(m)\right|^2 - N_{\rm h}$$
$$\hat{S}_{\rm v} = \frac{1}{M}\sum_{m=0}^{M-1}\left|\int_\Omega dV_{\rm v}(\mathbf{r},m)\,d\Omega + n_{\rm v}(m)\right|^2 - N_{\rm v}$$
$$\hat{R}_{\rm hv}(0) = \frac{1}{M}\sum_{m=0}^{M-1}\left[\int_\Omega dV_{\rm h}(\mathbf{r},m)\,d\Omega + n_{\rm h}(m)\right]^*\left[\int_\Omega dV_{\rm v}(\mathbf{r},m)\,d\Omega + n_{\rm v}(m)\right]e^{j[\alpha_{\rm h}(m)-\alpha_{\rm v}(m)]}, \quad (25)$$

where $n_{\rm h}(m)$ and $n_{\rm v}(m)$ are the $m$th samples of noise voltages, while $N_{\rm h} = \langle|n_{\rm h}(m)|^2\rangle$ and $N_{\rm v} = \langle|n_{\rm v}(m)|^2\rangle$ are the mean noise powers in the H and V channels, respectively. For simplicity the noise effects are neglected in further analysis. Note that as the signal becomes weaker, the cross-coupling component of the $\hat{Z}_{\rm DR}$ bias is unlikely to change [as indicated by the simplified analysis in Ivić and Doviak (2016)]. As for the $|\hat{\rho}_{\rm hv}(0)|$ and $\hat{\phi}_{\rm DP}$ biases, as well as the standard deviations of all three polarimetric variables, further investigation is needed to assess the possible effects. The mathematical expectations are

$$\langle\hat{S}_{\rm h}\rangle = \frac{1}{M}\sum_{m=0}^{M-1}\int_\Omega\langle|dV_{\rm h}(\mathbf{r},m)|^2\rangle\,d\Omega$$
$$\langle\hat{S}_{\rm v}\rangle = \frac{1}{M}\sum_{m=0}^{M-1}\int_\Omega\langle|dV_{\rm v}(\mathbf{r},m)|^2\rangle\,d\Omega$$
$$\langle\hat{R}_{\rm hv}(0)\rangle = e^{j\beta}\frac{1}{M}\sum_{m=0}^{M-1}\int_\Omega\langle dV_{\rm h}^*(\mathbf{r},m)\,dV_{\rm v}(\mathbf{r},m)\rangle e^{j[\alpha_{\rm h}(m)-\alpha_{\rm v}(m)]}\,d\Omega. \quad (26)$$

Because $s_{ll}(m)$ from different $dV_6$ volumes are uncorrelated, so are the differential powers $dV_l(\mathbf{r}, m)$. As a result, the magnitude square of the integrals in (25) becomes integrals of magnitudes squared along the solid angle $d\Omega$ in (26). In the AHV mode, similar results can be shown by following (19).

The described model shows that the voltages received in H and V are a function of intrinsic bulk properties of scatterers [represented by $s'_{\rm hh}(m)$ and $s_{\rm vv}(m)$] weighted by the antenna copolar and cross-polar patterns. Because the cross-coupling bias in polarimetric variable estimates is also a function of intrinsic hydrometeor parameters (Zrnić et al. 2010), it is necessary to include this dependency in the bias evaluation method. Because $s'_{\rm hh}(m)$ and $s_{\rm vv}(m)$ represent sampled echo voltages from a collection of scatterers in every $dV_6$, they can be simulated by generating samples of the H and V having specified intrinsic bulk properties [as described in Zrnić (1975) and Galati and Pavan (1995)]. From (23) it is evident that $s'_{\rm hh}(m)$ and $s_{\rm vv}(m)$ can be combined with the complex radiation patterns to obtain $dV_l(\mathbf{r}, m)$. Consequently, the constructed samples account for the effects of the H and V co- and cross-polar patterns. Hence, with the spatial integration of the differential contributions, this approach (or model) supports the analysis of polarimetric variable biases and standard deviations using simulated time series. Furthermore, simulated and measured $F_{lp}$ can be used to produce realistic weather echo voltages that can be used to assess polarimetric radar performance. Next, the procedure for generating the time series is described.

## 3. Time series generation

The first step is to generate the $M$ H and V simulated time series matrices of size $N_\theta \times M_\phi$ equal to the number of data points in the H and V radiating element pattern matrices. Each simulated sample can serve as a scattering center for an antenna pattern data point. Then, the signal samples received in H and V from $m$th transmission in a dwell are constructed as

$$
\begin{aligned}
V_{\mathrm{h}}(m) = \sum_{n_\theta=0}^{N_\theta-1}\sum_{m_\phi=0}^{M_\phi-1} \{&[F_{\mathrm{th}}^{\mathrm{co}}(n_\theta,m_\phi)F_{\mathrm{rh}}^{\mathrm{co}}(n_\theta,m_\phi)s'_{\mathrm{hh}}(m,n_\theta,m_\phi) + F_{\mathrm{th}}^{\mathrm{x}}(n_\theta,m_\phi)F_{\mathrm{rh}}^{\mathrm{x}}(n_\theta,m_\phi)s_{\mathrm{vv}}(m,n_\theta,m_\phi)]A_{\mathrm{h}}(m)e^{j\alpha_{\mathrm{h}}(m)} \\
&+ [F_{\mathrm{tv}}^{\mathrm{x}}(n_\theta,m_\phi)F_{\mathrm{rh}}^{\mathrm{co}}(n_\theta,m_\phi)s'_{\mathrm{hh}}(m,n_\theta,m_\phi) + F_{\mathrm{tv}}^{\mathrm{co}}(n_\theta,m_\phi)F_{\mathrm{rh}}^{\mathrm{x}}(n_\theta,m_\phi)s_{\mathrm{vv}}(m,n_\theta,m_\phi)]A_{\mathrm{v}}(m)e^{j[\beta+\alpha_{\mathrm{v}}(m)]}\} \\
&\times \sqrt{\sin[\Theta(n_\theta,m_\phi)]\Delta\theta\Delta\phi} \\
V_{\mathrm{v}}(m) = \sum_{n_\theta=0}^{N_\theta-1}\sum_{m_\phi=0}^{M_\phi-1} \{&[F_{\mathrm{tv}}^{\mathrm{x}}(n_\theta,m_\phi)F_{\mathrm{rv}}^{\mathrm{x}}(n_\theta,m_\phi)s'_{\mathrm{hh}}(m,n_\theta,m_\phi) + F_{\mathrm{tv}}^{\mathrm{co}}(n_\theta,m_\phi)F_{\mathrm{rv}}^{\mathrm{co}}(n_\theta,m_\phi)s_{\mathrm{vv}}(m,n_\theta,m_\phi)]A_{\mathrm{v}}(m)e^{j[\beta+\alpha_{\mathrm{v}}(m)]} \\
&+ [F_{\mathrm{th}}^{\mathrm{co}}(n_\theta,m_\phi)F_{\mathrm{rv}}^{\mathrm{x}}(n_\theta,m_\phi)s'_{\mathrm{hh}}(m,n_\theta,m_\phi) + F_{\mathrm{th}}^{\mathrm{x}}(n_\theta,m_\phi)F_{\mathrm{rv}}^{\mathrm{co}}(n_\theta,m_\phi)s_{\mathrm{vv}}(m,n_\theta,m_\phi)]A_{\mathrm{h}}(m)e^{j\alpha_{\mathrm{h}}(m)}\} \\
&\times \sqrt{\sin[\Theta(n_\theta,m_\phi)]\Delta\theta\Delta\phi}.
\end{aligned}
\tag{27}
$$

Note that the square root of $\sin[\Theta(n_\theta, m_\phi)]\Delta\theta\Delta\phi$ is added for convenience so that when second-order estimates [as in (13) and (19)] are computed, the dependency on the solid angle $d\Omega$ [as shown in (26)] is embedded in these estimates. This allows for the manipulation of the simulated time series in the same manner as those from the real radar. Simulated time series $s'_{\mathrm{hh}}(m, n_\theta, m_\phi)$ and $s_{\mathrm{vv}}(m, n_\theta, m_\phi)$ at every location can be assigned any parameters so the beams can be populated with scatterers of various bulk properties. Symbols $\Delta\theta$ and $\Delta\phi$ denote the resolution of antenna pattern data,

$$
\begin{aligned}
\Delta\theta &= |\Phi(n_\theta+1, m_\phi) - \Phi(n_\theta, m_\phi)| \\
\Delta\phi &= |\Theta(n_\theta, m_\phi+1) - \Theta(n_\theta, m_\phi)|,
\end{aligned}
\tag{28}
$$

where $\Phi(n_\theta, m_\phi)$ and $\Theta(n_\theta, m_\phi)$ are the matrices with $\theta$ and $\phi$ positions of data points in antenna patterns corresponding to $F_{lp}(n_\theta, m_\phi)$. Assuming no noise effects, each instantaneous second-order estimate is computed using (13) and (19) in the SHV and AHV modes, respectively.

## 4. Error estimation using realistic antenna patterns

In this section, an evaluation of the biases and standard deviations using realistic antenna patterns is presented. The patterns are generated using simulations based on the design from Massachusetts Institute of Technology (MIT) Lincoln Laboratory (Conway et al. 2013), which uses differential-fed single radiating elements. The antenna contains 10 panels arranged in a $2 \times 5$ matrix. Each panel consists of an $8 \times 8$ matrix of radiating elements. Such an arrangement results in a $7° \times 3°$ beamwidth at broadside. The operating frequency band of the antenna is 2.7–2.9 GHz. A dual-polarization phased array mobile radar based on these specifications has been built and delivered to the National Severe Storms Laboratory (NSSL) by the MIT Lincoln Laboratory (Ivić and Byrd 2015). It is used for evaluating the suitability of polarimetric phased array radar (PPAR) technology for weather applications as part of the MPAR effort led by NSSL.

The H and V co- and cross-polar patterns of a single radiating element $F_{lp}(n_\theta, m_\phi)$ [Fig. 2—where $l$ and $p$ are h or v, and $p$ denotes the excited T/R element port, while $l$ is the transmitted field orientation (Zrnić et al. 2010)]—were produced for the operating frequency of 2.85 GHz using the high-frequency structural simulator (HFSS), a commercial finite-element method solver for electromagnetic structures from ANSYS Inc. Figures 2e and 2g show that the one-way cross-polar pattern powers in both H and V are below −60 dB along principal planes but increase significantly at other locations. This indicates that measurement biases increase as the beam is steered away from principal planes. Furthermore, the difference in arguments of cross-polar patterns (Figs. 2f and 2h) between the two quadrants of interest (i.e., negative vs

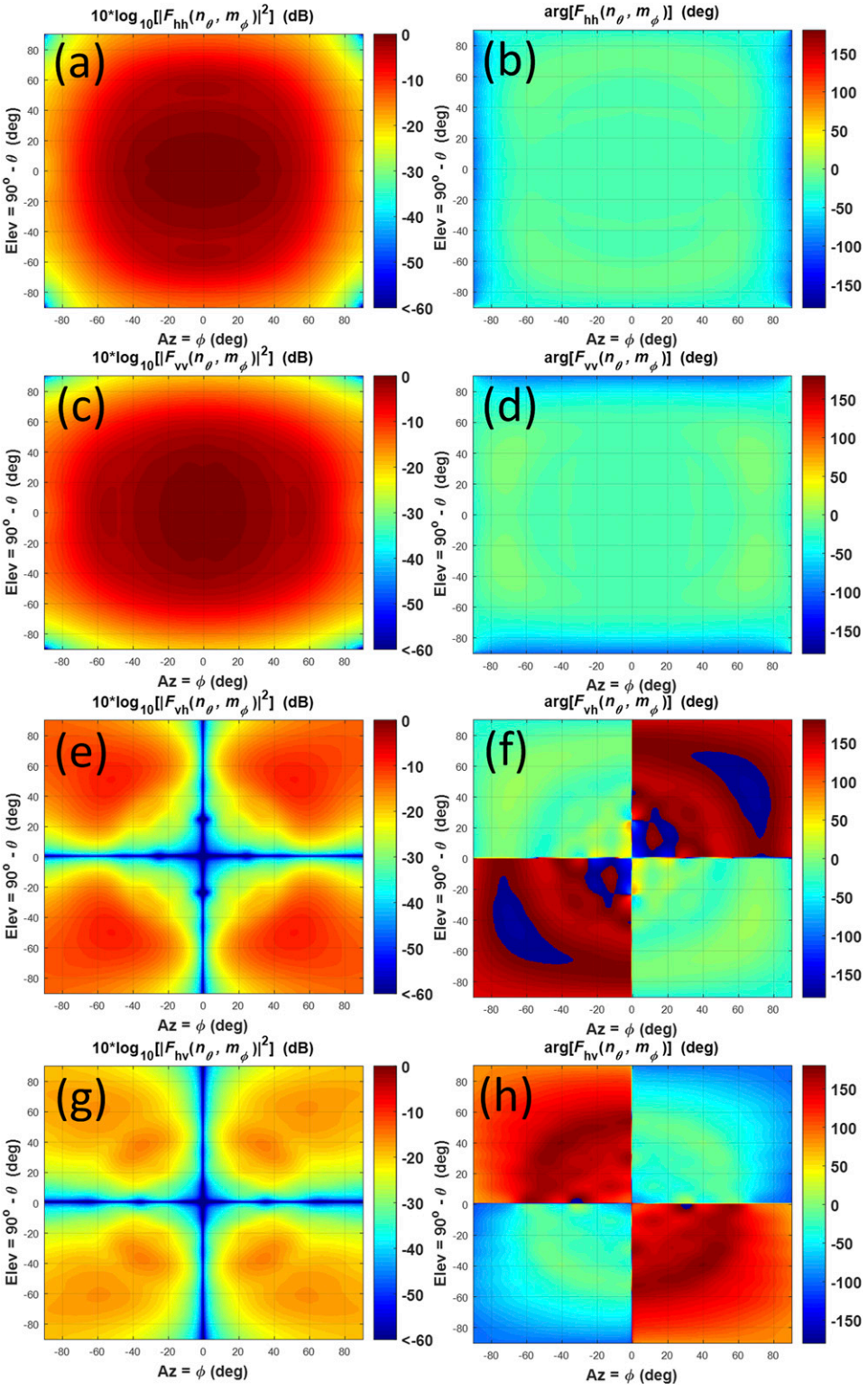


FIG. 2. One-way copolar patterns of a single radiating element in (a), (b) H and (c), (d) V. One-way cross-polar patterns of a single radiating element in (e), (f) H and (g), (h) V.

positive azimuths) indicates that the cross-coupling contributions to the bias and standard deviation are not symmetric around 0° azimuth. To obtain the patterns of the 10-panel array, $F_{lp}(n_\theta, m_\phi)$ were combined with the transmit and receive array factors in H and V (denoted as $AF_{ql}$, where $q$ is t or r and $l$ is h or v) as

$$\begin{aligned}
F_{tl}^{\mathrm{co}}(n_\theta, m_\phi) &= F_{ll}(n_\theta, m_\phi) AF_{tl}(n_\theta, m_\phi) \\
&= F_{ll}(n_\theta, m_\phi) \sum_{n_x=0}^{N_x-1} \sum_{m_y=0}^{M_y-1} W_{tl}(n_x, m_y) e^{j\{n_x[u(n_\theta,m_\phi)-u_0]+m_y[v(n_\theta,m_\phi)-v_0]\}} \\
F_{rl}^{\mathrm{co}}(n_\theta, m_\phi) &= F_{ll}(n_\theta, m_\phi) AF_{rl}(n_\theta, m_\phi) \\
&= F_{ll}(n_\theta, m_\phi) \sum_{n_x=0}^{N_x-1} \sum_{m_y=0}^{M_y-1} W_{rl}(n_x, m_y) e^{j\{n_x[u(n_\theta,m_\phi)-u_0]+m_y[v(n_\theta,m_\phi)-v_0]\}} \\
F_{q\mathrm{h}}^{\mathrm{x}}(n_\theta, m_\phi) &= F_{\mathrm{vh}}(n_\theta, m_\phi) AF_{q\mathrm{h}}(n_\theta, m_\phi) \\
&= F_{\mathrm{vh}}(n_\theta, m_\phi) \sum_{n_x=0}^{N_x-1} \sum_{m_y=0}^{M_y-1} W_{q\mathrm{h}}(n_x, m_y) e^{j\{n_x[u(n_\theta,m_\phi)-u_0]+m_y[v(n_\theta,m_\phi)-v_0]\}} \\
F_{q\mathrm{v}}^{\mathrm{x}}(n_\theta, m_\phi) &= F_{\mathrm{hv}}(n_\theta, m_\phi) AF_{q\mathrm{v}}(n_\theta, m_\phi) \\
&= F_{\mathrm{hv}}(n_\theta, m_\phi) \sum_{n_x=0}^{N_x-1} \sum_{m_y=0}^{M_y-1} W_{q\mathrm{v}}(n_x, m_y) e^{j\{n_x[u(n_\theta,m_\phi)-u_0]+m_y[v(n_\theta,m_\phi)-v_0]\}},
\end{aligned} \tag{29}$$

where symbols $W_{ql}(n_x, m_y)$ denote the weights applied to each radiating element in H and V on transmit and receive. Also,

$$\begin{aligned}
u(n_\phi, m_\theta) &= \frac{2\pi d_x}{\lambda} \sin[\Theta(n_\theta, m_\phi)] \sin[\Phi(n_\theta, m_\phi)] \\
v(n_\phi, m_\theta) &= \frac{2\pi d_y}{\lambda} \cos[\Theta(n_\theta, m_\phi)] \\
u_0 &= \frac{2\pi d_x}{\lambda} \sin(\theta_0) \sin(\phi_0) \\
v_0 &= \frac{2\pi d_y}{\lambda} \cos(\theta_0),
\end{aligned} \tag{30}$$

where $\lambda$ is the wavelength, while $\theta_0$ and $\phi_0$ are the steering angles. The spacing between centers of adjacent radiating elements along the $x$ axis is $d_x = 0.483 \times \lambda$ and along the $y$ axis is $d_y = 0.483 \times \lambda$. An example of array patterns for $\theta_0 = 70°$ (or for an elevation of 20°) and $\phi_0 = 40°$ are presented in Figs. 3 and 4. Note that the approach to pattern simulation used here does not account for the array effects (e.g., mutual couplings among adjacent radiating elements and radiating impedance of the array). Alternatively, the presented approach may produce more accurate antenna patterns if active (or embedded) element patterns (Pozar 1994; Mailloux 2005), which account for the array effects, are available (e.g., via measurements). This, however, is of no consequence, as the main objective herein is to introduce the method that evaluates the polarimetric variable biases due to co- and cross-polar patterns; hence, the patterns given here are used only for demonstrating the method. Nonetheless, an in-depth evaluation of errors using presented radiation patterns can provide valuable insight into the behavior of biases and standard deviations, as the beam is electronically steered in various directions. In both channels, transmit co- and cross-polar patterns exhibit higher sidelobes but narrower main beams compared to the receive patterns because the taper using a Taylor window was applied on receive but not on transmit.

### a. Bias estimation

Assuming uniformly distributed oblate scatterers of the same bulk properties so that SNR = Infinity (i.e., no noise is present so that SNR is infinite), and $|\rho_{\mathrm{hv}}(0)| = 0.98$ everywhere within the H and V antenna beams, the time series were generated using (27). The biases of the polarimetric variables were estimated using simulated time series as

$$\begin{aligned}
\mathrm{BIAS}\ \hat{Z}_{\mathrm{DR}} &= \frac{1}{K} \sum_{k=0}^{K-1} \hat{Z}_{\mathrm{DR}}^{k} - Z_{\mathrm{DR}} \\
\mathrm{BIAS}\ |\hat{\rho}_{\mathrm{hv}}(0)| &= \frac{1}{K} \sum_{k=0}^{K-1} |\hat{\rho}_{\mathrm{hv}}^{k}(0)| - |\rho_{\mathrm{hv}}(0)| \\
\mathrm{BIAS}\ \hat{\phi}_{\mathrm{DP}} &= \frac{1}{K} \sum_{k=0}^{K-1} \arg[\hat{\rho}_{\mathrm{hv}}^{k}(0)] - \phi_{\mathrm{DP}},
\end{aligned} \tag{31}$$

where $K$ designates the number of simulation realizations and the superscript $k$ denotes the realization

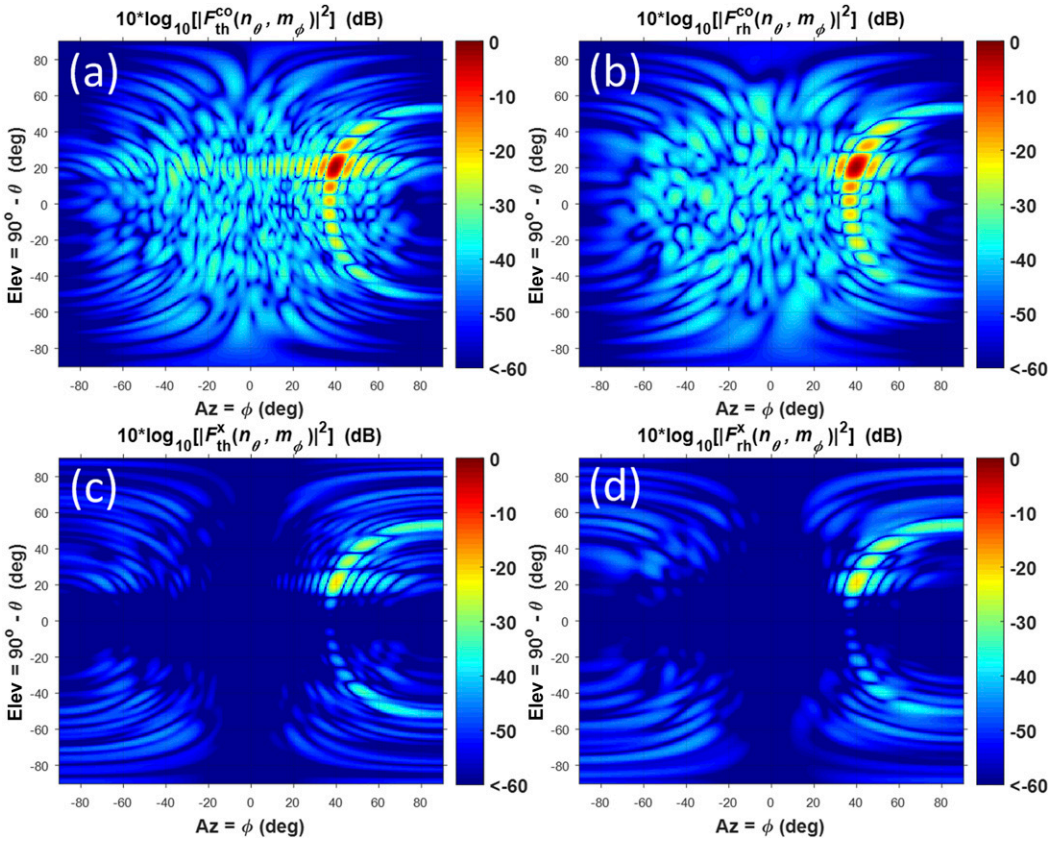


FIG. 3. One-way H copolar array power patterns for (a) transmit and (b) receive. One-way H cross-polar array power patterns on (c) transmit and (d) receive. Boresight is located at Elev = 20° and Az = 40°.

number. For comparison, the biases were also computed using analytical expressions (appendix A for the SHV mode and appendix B for the AHV mode).

Estimated biases due to the difference in copolar patterns (i.e., copolar biases) are presented in Fig. 5 if $Z_{DR}$ = 0 dB, and 5 dB for elevation (Elev) = 20° and azimuth (Az) = 40°. These biases vary, as the beam is electronically steered, and in real applications they must be corrected via a calibration procedure. Figure 5 also shows the biases caused by co- and cross-polar patterns (i.e., the sum of copolar and cross-coupling biases) as a function of intrinsic differential phase [because cross-coupling bias depends on $\phi_{DP}$; Zrnić et al. (2010)] for the nonphase and phase coded signals in the SHV mode (referred to as the SHV and PCSHV modes, respectively). The results are computed for the phase difference between the H and V transmit paths $\beta = 0°$. Note that the ensemble average of the phase difference between H and V measured from the received signals is a combination of the phase difference between the total transmit H and V patterns [given by the vector in (6)], $\phi_{DP}$, the phases of the receive co- and cross-polar H and V patterns, and the phase difference induced by the H and V receiver hardware. In reality, the biases in the polarimetric variable estimates are the sums of both copolar and cross-coupling biases and cannot be separated. The presented method, however, allows for the separate evaluation of these biases. In the case of $\hat{Z}_{DR}$ (Figs. 5a and 5d), the bias caused by the difference in copolar fields is constant for all $\phi_{DP}$ values, which is not the case for bias estimates due to co- and cross-polar fields [this is in agreement with the results presented in Zrnić et al. (2010)]. The biases from nonphase coded signals are visibly larger than those that are phase coded. This is expected, as the phase coding is designed to suppress the effects of cross coupling. If $Z_{DR}$ = 0 dB, then an agreement between the simulation and analytical results is very good (Fig. 5a). If $Z_{DR}$ = 5 dB (Fig. 5d), then the results from the simulation and the analytical derivations for the SHV mode, using Taylor series approximation [(A9)], start to differ, as the bias caused by co- and cross-polar patterns exceeds ~4 dB. The difference may be attributed to the Taylor series approximation employed to derive the $Z_{DR}$ bias expression (appendix A). On the other hand, the analytical results obtained using the direct formula [(A10)] agree well

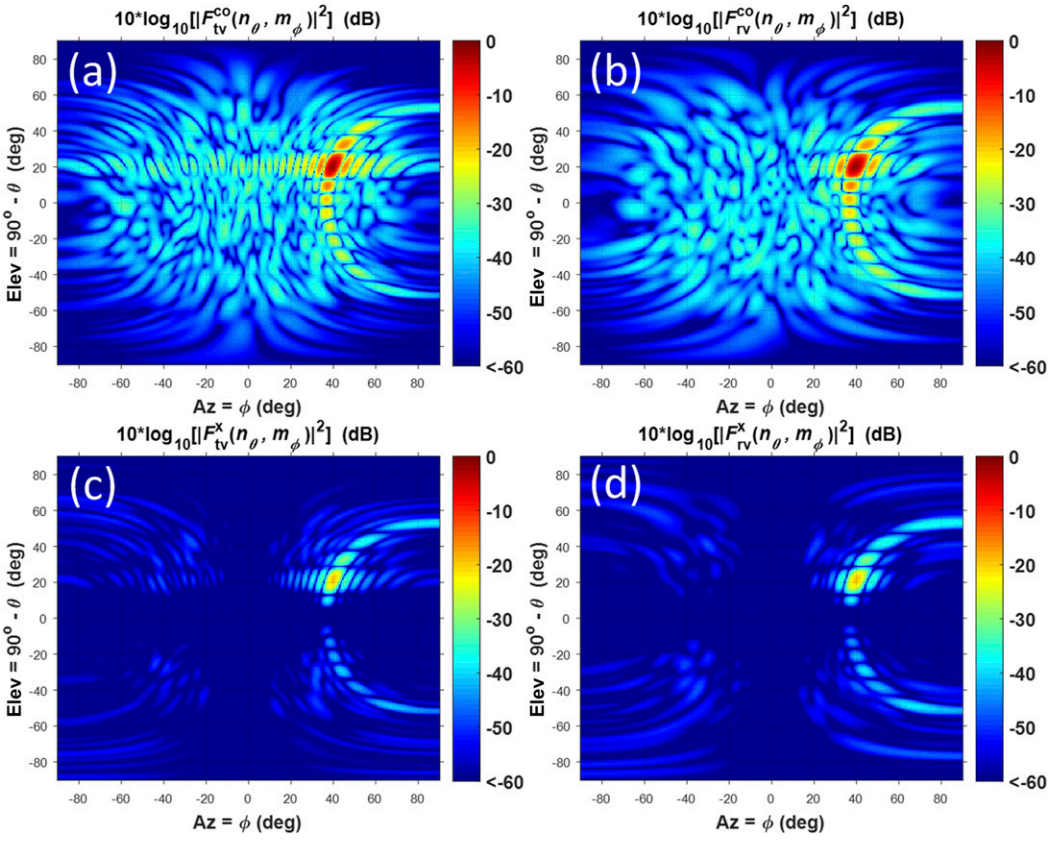


FIG. 4. One-way V copolar array power patterns on (a) transmit and (b) receive. One-way V cross-polar array power patterns on (c) transmit and (d) receive. Boresight is located at Elev = 20° and Az = 40°.

with the simulation in this case. If $Z_{DR} = 0$ dB, then the correlation coefficient biases (Fig. 5b) due to copolar fields do not differ excessively from those due to co- and cross-polar fields for nonphase coded signals, indicating that cross-polar fields induce bias smaller than ±0.01 (required for weather applications; Balakrishnan and Zrnić 1990) in the case shown. Also, simulation and analytical results agree reasonably in this case, even though the simulated bias exhibits more visible dependence on $\phi_{DP}$ for nonphase coded signals. If $Z_{DR} = 5$ dB (Fig. 5d), then the difference between the simulations and the analytical results, for nonphase coded signals, is significant, as the simulation shows this bias to exceed −0.01 for $\phi_{DP}$ values near 180° as opposed to the analytical computations. The discrepancy may be because the formulas for $\langle \hat{S}_h \rangle$, $\langle \hat{S}_v \rangle$, and $\langle |\hat{\rho}_{hv}(0)| \rangle$ do not include the cross-polar pattern terms higher than the second-order for simplicity. If this is indeed the case, it may be possible to obtain a more accurate formula for the $|\rho_{hv}(0)|$ bias by taking the higher-order cross-polar pattern terms into account (further investigation into this is beyond the scope of this paper and is more suited for future research). In both cases, the simulation and analytical results for $|\hat{\rho}_{hv}(0)|$ bias of phase coded signals agree well. This may be the consequence of the phase code application, which cancels some of the higher-order cross-polar terms, which results in better agreement between the two results. Also, both the simulation and analytical results show an increase in the $|\hat{\rho}_{hv}(0)|$ bias from phase coded signals for the two cases shown. This indicates that while the phase coding method mitigates the $\hat{Z}_{DR}$ bias, it may exacerbate the errors in the correlation coefficient estimates. In the case of $\phi_{DP}$ estimates (Figs. 5c and 5f), the bias due to copolar fields is constant for all $\phi_{DP}$ values but this is not the case for bias estimates due to co- and cross-polar fields (i.e., in the SHV and PCSHV modes). For instance, the curves in Fig. 5f show that, for the given case, the $\hat{\phi}_{DP}$ bias is ~3.5° if $\phi_{DP} = 0°$ (e.g., as H and V fields enter the space filled with hydrometeors) in both the SHV and PCSHV modes. The same curves show that as fields propagate through a range extent populated by scatterers, the difference between the SHV and PCSHV $\hat{\phi}_{DP}$ biases increases so that if $\phi_{DP} = 100°$, then the corresponding $\hat{\phi}_{DP}$ bias is −12° in the SHV mode and −1.1° in the PCSHV mode. The simulation and analytical results

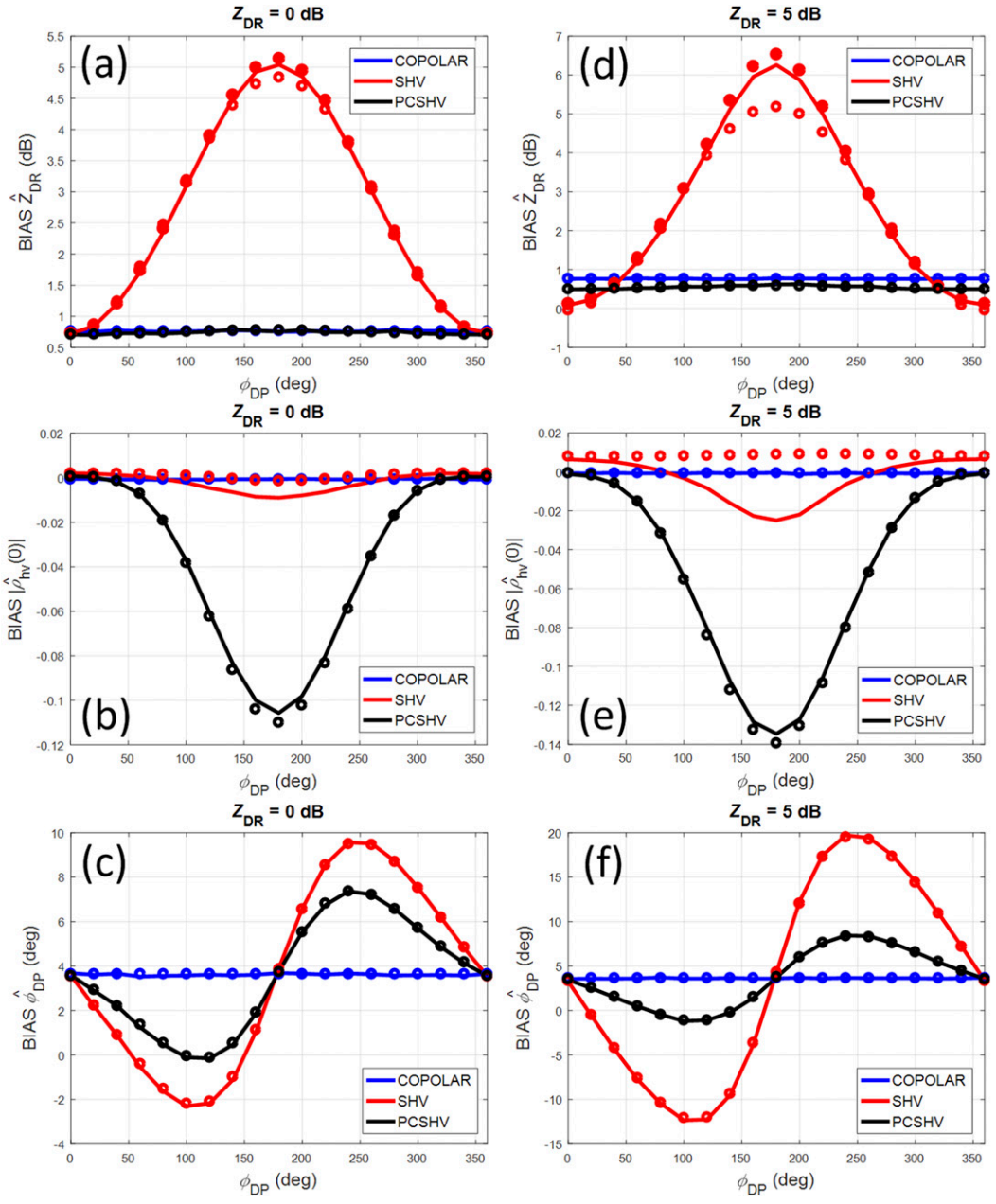


FIG. 5. Estimated (solid lines) and analytical (circles) bias for SHV and PCSHV modes vs $\phi_{DP}$ if $Z_{DR} = 0$ dB for (a) $\hat{Z}_{DR}$ [using Taylor series (circles) and computed directly (solid dots)], (b) $|\hat{\rho}_{hv}(0)|$, and (c) $\hat{\phi}_{DP}$; and if $Z_{DR} = 5$ dB for (d) $\hat{Z}_{DR}$ [using Taylor series (circles) and computed directly (solid dots)], (e) $|\hat{\rho}_{hv}(0)|$, and (f) $\hat{\phi}_{DP}$. Boresight is located at Elev = 20° and Az = 40°.

agree well for both $Z_{DR} = 0$ dB and $Z_{DR} = 5$ dB, showing the reduced bias for phase coded signals.

The performance of the AHV mode without the presence of cross coupling was analyzed in Melnikov and Zrnić (2015). Therein, it is shown that for the unambiguous velocity $v_a$ of $\sim 9\,\mathrm{m\,s^{-1}}$, the estimates of differential reflectivity are unbiased, whereas the estimates of differential phase and copolar correlation coefficient exhibit strong biases. This is because the estimators of $|\rho_{hv}(0)|$ and $\phi_{DP}$ in the AHV mode use the estimates of correlations in sample time. Furthermore, Melnikov and Zrnić (2015) demonstrated that the standard deviations of the estimates in the AHV mode are much larger than in the SHV mode if $v_a = \sim 9\,\mathrm{m\,s^{-1}}$

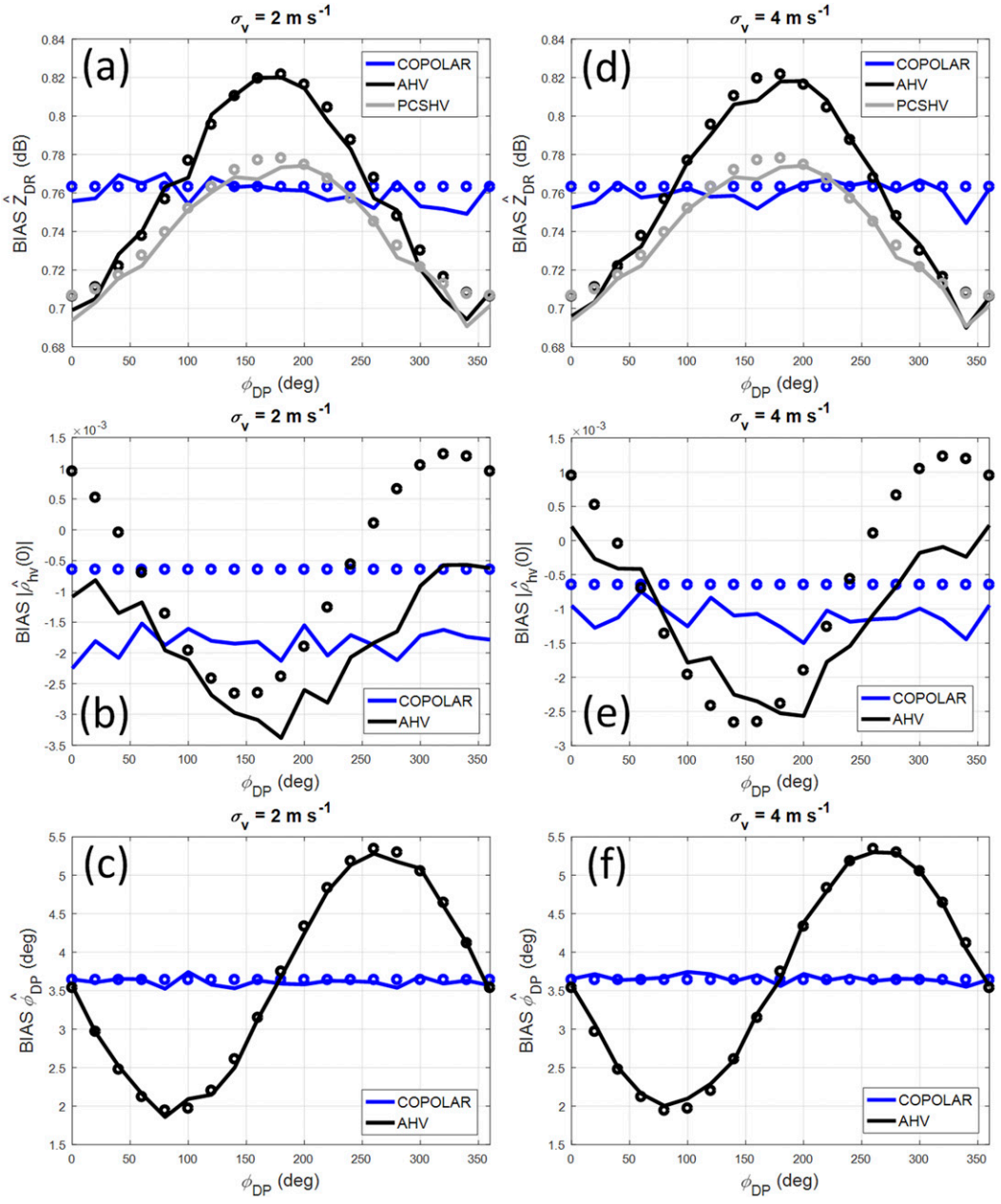


FIG. 6. Estimated (solid lines) and analytical (circles) bias for AHV mode if SNR = Inf, $v_a = 30\,\mathrm{m\,s^{-1}}$, $M = 32$, $Z_{\mathrm{DR}} = 0\,\mathrm{dB}$ vs $\phi_{\mathrm{DP}}$ if $\sigma_v = 2\,\mathrm{m\,s^{-1}}$ for (a) $\hat{Z}_{\mathrm{DR}}$, (b) $|\hat{\rho}_{\mathrm{hv}}(0)|$, and (c) $\hat{\phi}_{\mathrm{DP}}$; and if $\sigma_v = 4\,\mathrm{m\,s^{-1}}$ for (d) $\hat{Z}_{\mathrm{DR}}$, (e) $|\hat{\rho}_{\mathrm{hv}}(0)|$, and (f) $\hat{\phi}_{\mathrm{DP}}$. Boresight is located at Elev = 20° and Az = 40°.

(due to temporal decorrelation effects). This suggests that the application of the AHV mode for scans with $v_a$ on the order of $9\,\mathrm{m\,s^{-1}}$ is not recommended. Accordingly, the results for the AHV mode are produced for $v_a = 30\,\mathrm{m\,s^{-1}}$. For this case, the analysis in Melnikov and Zrnić (2015) indicates that the AHV and SHV modes produce comparable performances if a spectrum width is less than about $4\,\mathrm{m\,s^{-1}}$ (at S band), but the performance of the AHV mode degrades rapidly at wider widths. Consequently, the bias results in the AHV mode are plotted for $\sigma_v$ of 2 and $4\,\mathrm{m\,s^{-1}}$ (Fig. 6).

The results presented in Fig. 6 show the biases of the polarimetric variable estimates in the AHV mode to be almost the same for $\sigma_v$ of 2 and $4\,\mathrm{m\,s^{-1}}$. For comparison, the $\hat{Z}_{\mathrm{DR}}$ biases in the PCSHV mode are also shown in Figs. 6a and 6d (as these are obscured by the large biases in the SHV mode in Fig. 5a). The plots indicate that the cross-coupling biases in the PCSHV mode are to some

extent smaller than those in the AHV mode for the cases shown (assuming the proper correction of the copolar bias via calibration). For $|\hat{\rho}_{hv}(0)|$, the biases are insignificant (Figs. 6b and 6e) and are much smaller than in the PCSHV mode. For $\hat{\phi}_{DP}$, the AHV mode exhibits ~3.5° bias change with $\phi_{DP}$ compared to the ~7.5° in the PCSHV mode for the cases shown (Figs. 6c and 6f, as well as Fig. 5c).

*b. Standard deviation estimation*

As in the case of bias, uniformly distributed oblate scatterers of the same bulk properties, so $Z_{DR} = 0$ dB and $|\rho_{hv}(0)| = 0.98$ everywhere within the H and V antenna beams, were assumed. Note that unlike bias in SHV and PCSHV modes, the standard deviation of the polarimetric variable estimates depends on $M$ and $\sigma_v$ as well as $v_a$. The standard deviations (std dev) of the polarimetric variables were estimated using simulated time series as

$$\text{Std dev } \hat{Z}_{DR} = \sqrt{\frac{1}{K}\sum_{k=0}^{K-1}\left[\hat{Z}_{DR}^{k} - \frac{1}{K}\sum_{l=0}^{K-1}\hat{Z}_{DR}^{l}\right]^2}$$

$$\text{Std dev } |\hat{\rho}_{hv}(0)| = \sqrt{\frac{1}{K}\sum_{k=0}^{K-1}\left[|\hat{\rho}_{hv}^{k}(0)| - \frac{1}{K}\sum_{l=0}^{K-1}|\hat{\rho}_{hv}^{l}(0)|\right]^2}$$

$$\text{Std dev } \hat{\phi}_{DP} = \sqrt{\frac{1}{K}\left(\arg[\hat{\rho}_{hv}^{k}(0)] - \frac{1}{K}\sum_{l=0}^{K-1}\arg[\hat{\rho}_{hv}^{l}(0)]\right)^2}. \quad (32)$$

For the SHV mode, $v_a$ was set to 9 m s$^{-1}$ with $M = 16$ and 30 m s$^{-1}$ with $M = 32$, while the spectrum width was set to 2 and 4 m s$^{-1}$. The results for the nonphase and phase coded signals are plotted in Figs. 7 and 8, for $v_a$ of 9 and 30 m s$^{-1}$, respectively. For reference, the results produced using only copolar signals are presented as well. As with bias, the standard deviations of the nonphase and phase coded signals are dependent on $\phi_{DP}$ variations, while those from the copolar signals are not. This clearly indicates that the $\phi_{DP}$ dependence is imposed by the presence of cross-polar fields. If $v_a = 9$ m s$^{-1}$ and $\sigma_v = 4$ m s$^{-1}$, then the $\hat{Z}_{DR}$ and $|\hat{\rho}_{hv}(0)|$ standard deviations of the nonphase coded signals are appreciably smaller than those produced from phase coded signals (Figs. 7d and 7e) but if $\sigma_v = 2$ m s$^{-1}$, the standard deviations in both SHV and PCSHV modes are comparable (Figs. 8a and 8b). For $\hat{\phi}_{DP}$, the standard deviations from the phase coded signals are smaller than from the nonphase coded signals (Figs. 7c and 7f) for both $\sigma_v$ values. If $v_a = 30$ m s$^{-1}$ (Fig. 8), then the standard deviations in the PCSHV mode are always smaller than in the SHV mode. In case of $\hat{Z}_{DR}$, the analytical derivations for standard deviations are given in Ivić and Doviak (2016) for the case when the transmit and receive fields are equal (i.e., $F_{th}^{co} = F_{rh}^{co} = F_{hh}$, $F_{tv}^{co} = F_{rv}^{co} = F_{vv}$, $F_{th}^{x} = F_{rh}^{x} = F_{vh}$, $F_{tv}^{x} = F_{rv}^{x} = F_{hv}$), and each field is described by a single complex number (see Eqs. (39) and (42) in Ivić and Doviak). Because of the multiple Taylor series expansions and approximations, the expressions in Ivić and Doviak (2016) do not reflect the standard deviation dependency on $\phi_{DP}$ as indicated by the simulation results presented herein. This demonstrates the benefit of the presented method for assessing the standard deviation of the polarimetric variable estimates in the presence of cross-polar fields.

The plots for the AHV mode standard deviations for SNR = Inf, $v_a = 30$ m s$^{-1}$, $M = 32$, and $Z_{DR} = 0$ dB are presented in Fig. 9 for $\sigma_v$ of 2 m s$^{-1}$ and 4 m s$^{-1}$. As opposed to the SHV and PCSHV modes, the standard deviations do not exhibit significant variation with $\phi_{DP}$. The ratios of AHV versus PCSHV mean standard deviations for all three polarimetric variables are given in Table 1. These show the AHV and PCSHV standard deviations to be comparable for $\hat{Z}_{DR}$ and $\hat{\phi}_{DP}$ (with a slight ratio increase with $\sigma_v$) but not for $|\hat{\rho}_{hv}(0)|$, where the estimates in the AHV mode exhibited 31% and 52% larger standard deviations for $\sigma_v$ of 2 m s$^{-1}$ and 4 m s$^{-1}$, respectively.

## 5. Summary and conclusions

A method to evaluate the biases and standard deviations of polarimetric variable estimates using measured or simulated co- and cross-polar antenna patterns combined with simulated time series is presented. Because it does not use approximations commonly employed by the analytical computations, it can be used for the verification of analytically obtained results or independently. The main goal was to develop the method applicable to the phased array antennas. Therefore, the previously developed model describing the echo voltages received by the parabolic reflector antenna is updated to accommodate the specifics of phased array antennas. This is because this model assumed that the co- and cross-polar radiation patterns in H and V on transmit and receive were equal, which is true for parabolic antennas but generally not for phased array systems due to the beamforming weights applied to single radiating elements on transmit and/or receive. Accordingly, different radiation matrices are used to describe transmit and receive copolar and cross-polar patterns in H and V. To provide theoretical background for simulation, a generally used concept where the backscattering matrix describes the backscattering properties of a single hydrometeor is modified whereby the properties of a collection of scatterers (contained in a resolution volume of arbitrary size) are described by the backscattering matrix (in the absence of depolarization

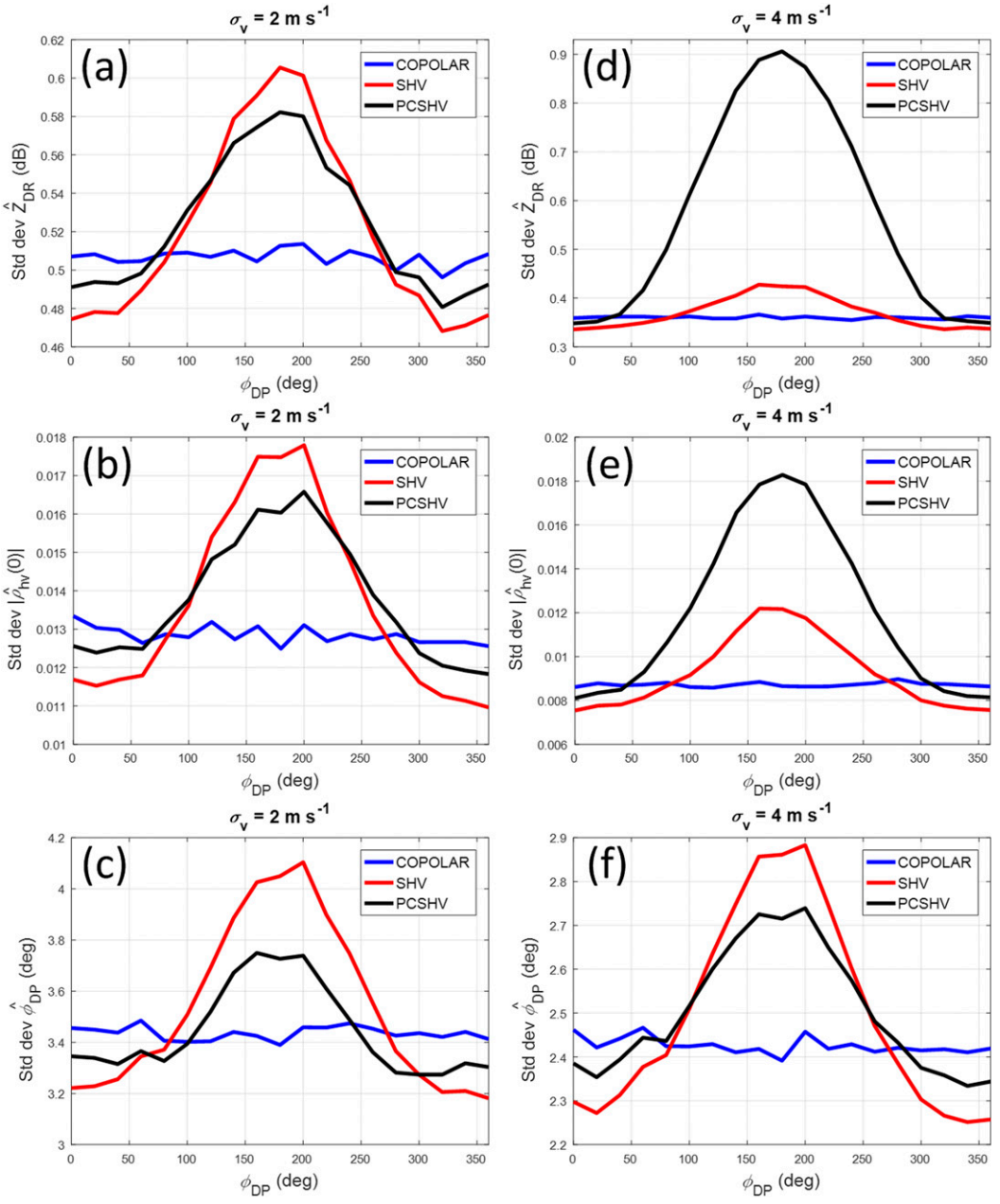


FIG. 7. Estimated std dev in the SHV and PCSHV modes for SNR = Inf, $v_a = 9\,\mathrm{m\,s^{-1}}$, $M = 16$, $Z_{DR} = 0\,\mathrm{dB}$, $|\rho_{hv}(0)| = 0.98$ vs $\phi_{DP}$ if $\sigma_v = 2\,\mathrm{m\,s^{-1}}$ for (a) $\hat{Z}_{DR}$, (b) $|\hat{\rho}_{hv}(0)|$, and (c) $\hat{\phi}_{DP}$; and if $\sigma_v = 4\,\mathrm{m\,s^{-1}}$ for (d) $\hat{Z}_{DR}$, (e) $|\hat{\rho}_{hv}(0)|$, and (f) $\hat{\phi}_{DP}$. Boresight is located at Elev = 20° and Az = 40°.

by the scattering media). Elements of such modified backscattering matrix account for the replacement of scatterers within the resolution volume between subsequent transmissions as well as the fact that scatterers have different relative ranges upon every illumination. Also, the fact that the wobbling and oscillations of scatterers within the resolution volume produce slight decorrelation between the H and V matrix elements resulting in $|\rho_{hv}(0)|$ values below one is accounted for. Consequently, voltages, obtained using elements of the modified backscattering matrix, have random real and imaginary parts that are zero mean and Gaussian distributed functions of time between transmissions. Thus, a so defined modified backscattering matrix describes the bulk statistical properties of particles within a resolution volume over the radar dwell time. Statistical properties

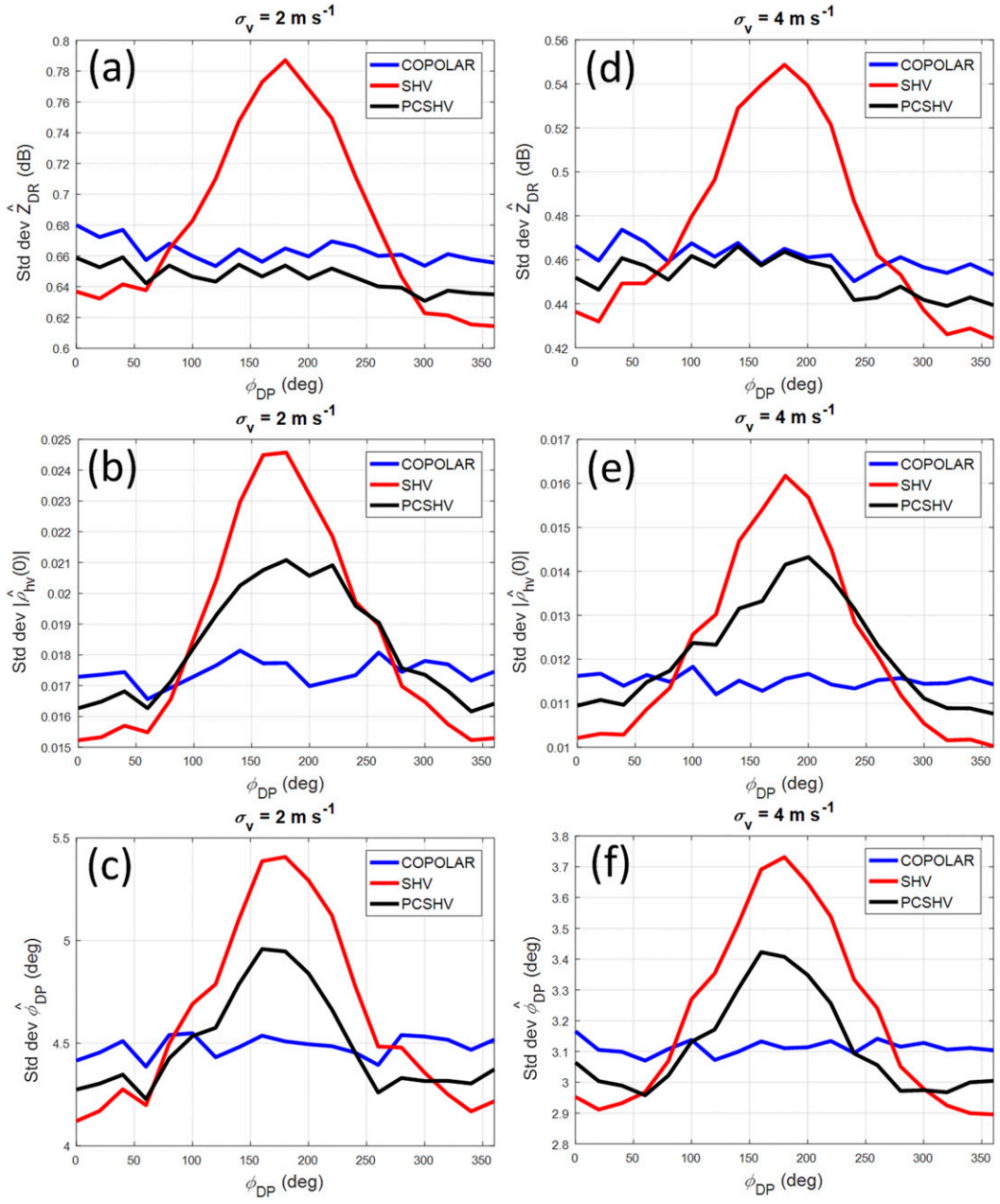


FIG. 8. Estimated std dev in the SHV and PCSHV modes for SNR = Inf, $v_a = 30\,\mathrm{m\,s^{-1}}$, $M = 32$, and $Z_{DR} = 0$ dB vs $\phi_{DP}$ if $\sigma_v = 2\,\mathrm{m\,s^{-1}}$ for (a) $\hat{Z}_{DR}$, (b) $|\hat{\rho}_{hv}(0)|$, and (c) $\hat{\phi}_{DP}$; and if $\sigma_v = 4\,\mathrm{m\,s^{-1}}$ for (d) $\hat{Z}_{DR}$, (e) $|\hat{\rho}_{hv}(0)|$, and (f) $\hat{\phi}_{DP}$. Boresight is located at Elev = 20° and Az = 40°.

of the modified backscattering matrix elements are described by the radar observables. Consequently, the elements of this matrix can be simulated using well-established methods.

Based on the specified bulk properties of scatterers, instantaneous realizations of modified backscattering matrix values are produced for each unit resolution volume in space (set equal to the resolution of the radiation patterns in azimuth and elevation). These values are weighted by the corresponding co- and cross-polar radiation pattern values and summed to produce time series. So, obtained time series account for the effects of co- and cross-polar fields specific to the antenna used to produce the patterns and allow for the assessment of biases caused by these radiation patterns, as well as the standard deviation of estimates. Furthermore,

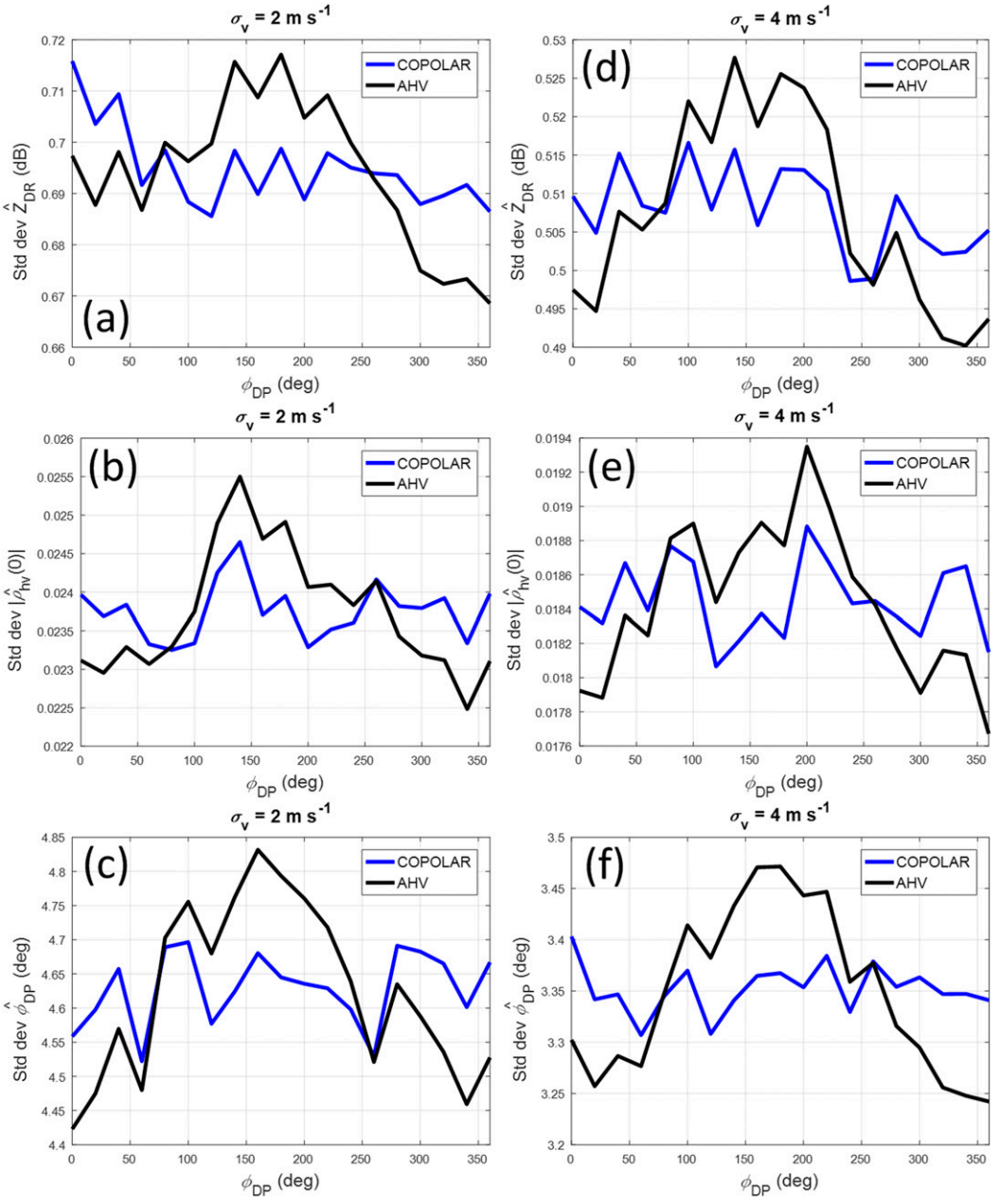


FIG. 9. Estimated std dev in the AHV mode for SNR = Inf, $v_a = 30\,\mathrm{m\,s^{-1}}$, $M = 32$, and $Z_{DR} = 0$ dB vs $\phi_{DP}$ if $\sigma_v = 2\,\mathrm{m\,s^{-1}}$ for (a) $\hat{Z}_{DR}$, (b) $|\hat{\rho}_{hv}(0)|$, and (c) $\hat{\phi}_{DP}$; and if $\sigma_v = 4\,\mathrm{m\,s^{-1}}$ for (d) $\hat{Z}_{DR}$, (e) $|\hat{\rho}_{hv}(0)|$, and (f) $\hat{\phi}_{DP}$. Boresight is located at Elev = 20° and Az = 40°.

because the radar field of view can be populated with particles of varying properties, the method can be used to investigate the effects of nonuniformities within the radar beam on weather observations. Furthermore, the method provides for the separation of the effects of copolar and cross-polar fields. Consequently, the biases and standard deviations of signals from copolar fields can be evaluated separately from those caused by cross-polar fields and vice versa. This contrasts with the time series obtained from actual radar (i.e., real time series), where the effects of co- and cross-polar fields cannot be separated.

The method was demonstrated using array patterns produced by combining the simulated single element radiating patterns with the array factor. These patterns do not account for the array effects (e.g., the mutual coupling among individual elements, the manufacturing uncertainties, and the radiating impedance of the array)

TABLE 1. Ratio of AHV to PCSHV mean std dev for SNR = Inf, $v_a = 30\,\mathrm{m\,s^{-1}}$, $M = 32$, and $Z_{DR} = 0\,\mathrm{dB}$.

| AHV-to-PCSHV mean std dev ratio | $\sigma_v = 2\,\mathrm{m\,s^{-1}}$ | $\sigma_v = 4\,\mathrm{m\,s^{-1}}$ |
|---|---|---|
| $\hat{Z}_{DR}$ | 1.07 | 1.12 |
| $\lvert\hat{\rho}_{hv}(0)\rvert$ | 1.31 | 1.52 |
| $\hat{\phi}_{DP}$ | 1.03 | 1.06 |

and other hardware mechanisms that contribute to cross-polar fields (e.g., coupling through circuits behind the antenna backplane). Thus, to obtain more accurate bias and standard deviation estimates, the use of measured or simulated patterns that account for the array effects is preferable. If the patterns are sufficiently accurate, these may be used for bias correction in the polarimetric variable estimates produced from real time series.

To provide an example of the technique's effectiveness for bias computations in the SHV mode, the radar field of view was populated with oblate scatterers of the same bulk properties for $Z_{DR}$ values of 0 and 5 dB. Next, the biases of nonphase and phase coded signals for all three polarimetric variables were estimated for array patterns obtained by steering the beam to the azimuth of 40° and elevation of 20°. For comparison, the bias results obtained using analytical expressions were also presented. As expected biases due to copolar fields showed no significant variations with changing $\phi_{DP}$ values. Contrary to this, the biases caused by co- and cross-polar fields exhibited visible dependence on $\phi_{DP}$. The simulation and analytical results matched well for copolar biases. In the case of the biases caused by the cross coupling, the following was obtained for nonphase coded signals in the SHV mode. For a $Z_{DR}$ of 0 dB, the simulation and analytical results matched well but exhibited noticeable differences for a $Z_{DR}$ of 5 dB in the case of $\hat{Z}_{DR}$ bias (if derived using Taylor series expansion) and the $|\hat{\rho}_{hv}(0)|$ bias. In the case of $\hat{Z}_{DR}$ bias, the differences are attributed to the Taylor series approximations employed to derive the $\hat{Z}_{DR}$ bias expression. This is supported by the results obtained using the analytical $\hat{Z}_{DR}$ expression directly (i.e., without the Taylor series expansion) because these results agreed well with the simulation (for the cases shown). In the case of $|\hat{\rho}_{hv}(0)|$ bias, it was speculated that the difference was caused by the simplification of the second-order estimates used to compute the $|\hat{\rho}_{hv}(0)|$ bias. For phase coded signals, the simulation and analytical results agreed well for $\hat{Z}_{DR}$ and $|\hat{\rho}_{hv}(0)|$ biases. In the case of $\phi_{DP}$ bias, the analytical and simulation results also agreed well for both the nonphase and phase coded signals. In the AHV mode, the analytical and simulation results exhibited good agreement for all presented cases. In summary, the proposed method exhibited good agreement with the analytical results, thus demonstrating the validity of the approach.

The simulation results for standard deviation were presented for unambiguous velocities of 9 and $30\,\mathrm{m\,s^{-1}}$ for the SHV mode. In the first case, the results from phase coded signals, in the SHV mode, exhibited a significantly higher fluctuation of estimates than those from nonphase coded signals for $\hat{Z}_{DR}$ and $|\hat{\rho}_{hv}(0)|$ but not for $\hat{\phi}_{DP}$. If $v_a$ is $30\,\mathrm{m\,s^{-1}}$, then the estimates produced using phase codes demonstrated smaller standard deviations than those from nonphase coded signals. In the AHV mode, the results were produced for an unambiguous velocity of $30\,\mathrm{m\,s^{-1}}$ (because previous works demonstrated poor performance at $v_a$ of $9\,\mathrm{m\,s^{-1}}$). The results indicated comparable performance to the SHV mode for $\hat{Z}_{DR}$ and $\hat{\phi}_{DP}$ but a significant increase in $|\hat{\rho}_{hv}(0)|$ standard deviations. Because of the lack of proper analytical expressions and the complexity of their derivation, the standard deviations were evaluated using only simulations. This demonstrated the benefit of the presented method for evaluating the standard deviation of polarimetric variable estimates in the presence of cross-polar fields.

*Acknowledgments.* The author would like to thank Dr. Dušan S. Zrnić for his valuable comments and guidance, which enhanced this work. Also, the author would like to thank Kurt Hondl for providing comments, which improved the manuscript; and James Skala of Georgia Tech Research Institute (GTRI) for providing the HFSS simulations used in this work. Finally, the author would like to thank Henry Thomas of MIT Lincoln Laboratory for providing the MATLAB code used for the array factor simulation in this work. Funding was provided by NOAA/Office of Oceanic and Atmospheric Research under NOAA–University of Oklahoma Cooperative Agreement NA11OAR4320072, U.S. Department of Commerce.

## APPENDIX A

### Derivation of Analytical Bias Expressions for the SHV Mode

In this appendix a derivation of analytical formulas for the mathematical expectations of $\hat{Z}_{DR}$, $|\hat{\rho}_{hv}(0)|$, and $\hat{\phi}_{DP}$ in the SHV mode is presented. The derivation is used to produce the theoretical bias expressions. The formulas are derived by following the model, which uses $\mathbf{S}$, introduced in the text.

The received powers after each transmission in the H and V channels are

$$
\begin{aligned}
|V_{\mathrm{h}}(\mathbf{r},m)|^2 &= \left|\int_{\Omega} dV_{\mathrm{h}}(\mathbf{r},m)\,d\Omega\right|^2,\\
&= \int_{\Omega} |dV_{\mathrm{h}}(\mathbf{r},m)|^2\,d\Omega + \underbrace{\int_{\Omega_1} dV_{\mathrm{h}}(\mathbf{r},m)\,d\Omega_1 \int_{\Omega_2} dV_{\mathrm{h}}(\mathbf{r},m)\,d\Omega_2}_{d\Omega_1 \neq d\Omega_2},\\
&= \int_{\Omega} [d\hat{S}_{\mathrm{h}}^{\mathrm{co}}(\Omega,m) + d\hat{S}_{\mathrm{h}}^{\mathrm{x}}(\Omega,m)]\,d\Omega + \underbrace{\int_{\Omega_1} dV_{\mathrm{h}}(\mathbf{r},m) d\Omega_1 \int_{\Omega_2} dV_{\mathrm{h}}(\mathbf{r},m)\,d\Omega_2}_{d\Omega_1 \neq d\Omega_2}.\\
|V_{\mathrm{v}}(\mathbf{r},m)|^2 &= \left|\int_{\Omega} dV_{\mathrm{v}}(\mathbf{r},m)\,d\Omega\right|^2,\\
&= \int_{\Omega} |dV_{\mathrm{v}}(\mathbf{r},m)|^2\,d\Omega + \underbrace{\int_{\Omega_1} dV_{\mathrm{v}}(\mathbf{r},m)\,d\Omega_1 \int_{\Omega_2} dV_{\mathrm{v}}(\mathbf{r},m)\,d\Omega_2}_{d\Omega_1 \neq d\Omega_2},\\
&= \int_{\Omega} [d\hat{S}_{\mathrm{v}}^{\mathrm{co}}(\Omega,m) + d\hat{S}_{\mathrm{v}}^{\mathrm{x}}(\Omega,m)]\,d\Omega + \underbrace{\int_{\Omega_1} dV_{\mathrm{v}}(\mathbf{r},m)\,d\Omega_1 \int_{\Omega_2} dV_{\mathrm{v}}(\mathbf{r},m)\,d\Omega_2}_{d\Omega_1 \neq d\Omega_2}, \qquad \text{(A1)}
\end{aligned}
$$

where

$$
\begin{aligned}
d\hat{S}_{\mathrm{h}}^{\mathrm{co}}(\Omega,m) &= |F_{\mathrm{th}}^{\mathrm{co}} F_{\mathrm{rh}}^{\mathrm{co}} s'_{\mathrm{hh}}(m)|^2\\
d\hat{S}_{\mathrm{h}}^{\mathrm{co}}(\Omega,m) &= |F_{\mathrm{tv}}^{\mathrm{co}} F_{\mathrm{rv}}^{\mathrm{co}} s_{\mathrm{vv}}(m)|^2\\
d\hat{S}_{\mathrm{h}}^{\mathrm{x}}(\Omega,m) &\approx |F_{\mathrm{tv}}^{\mathrm{x}}|^2 |F_{\mathrm{rh}}^{\mathrm{co}}|^2 |s'_{\mathrm{hh}}(m)|^2 + |F_{\mathrm{tv}}^{\mathrm{co}}|^2 |F_{\mathrm{rh}}^{\mathrm{x}}|^2 |s_{\mathrm{vv}}(m)|^2\\
&\quad + 2\mathrm{Re}\{F_{\mathrm{tv}}^{\mathrm{x}*} F_{\mathrm{rh}}^{\mathrm{co}*} F_{\mathrm{tv}}^{\mathrm{co}} F_{\mathrm{rh}}^{\mathrm{x}} s'^{*}_{\mathrm{hh}}(m) s_{\mathrm{vv}}(m) + F_{\mathrm{th}}^{\mathrm{co}*} F_{\mathrm{rh}}^{\mathrm{co}*} F_{\mathrm{th}}^{\mathrm{x}} F_{\mathrm{rh}}^{\mathrm{x}} s'^{*}_{\mathrm{hh}}(m) s_{\mathrm{vv}}(m)\}\\
&\quad + 2\mathrm{Re}\{[F_{\mathrm{th}}^{\mathrm{co}*} F_{\mathrm{rh}}^{\mathrm{co}*} F_{\mathrm{tv}}^{\mathrm{x}} F_{\mathrm{rh}}^{\mathrm{co}} |s'_{\mathrm{hh}}(m)|^2 + F_{\mathrm{th}}^{\mathrm{co}*} F_{\mathrm{rh}}^{\mathrm{co}*} F_{\mathrm{tv}}^{\mathrm{co}} F_{\mathrm{rh}}^{\mathrm{x}} s'^{*}_{\mathrm{hh}}(m) s_{\mathrm{vv}}(m)] e^{j[\beta+\alpha_{\mathrm{v}}(m)-\alpha_{\mathrm{h}}(m)]}\}\\
d\hat{S}_{\mathrm{v}}^{\mathrm{x}}(\Omega,m) &\approx |F_{\mathrm{th}}^{\mathrm{x}}|^2 |F_{\mathrm{rv}}^{\mathrm{co}}|^2 |s_{\mathrm{vv}}(m)|^2 + |F_{\mathrm{th}}^{\mathrm{co}}|^2 |F_{\mathrm{rv}}^{\mathrm{x}}|^2 |s'_{\mathrm{hh}}(m)|^2\\
&\quad + 2\mathrm{Re}\{F_{\mathrm{th}}^{\mathrm{x}*} F_{\mathrm{rv}}^{\mathrm{co}*} F_{\mathrm{th}}^{\mathrm{co}} F_{\mathrm{rv}}^{\mathrm{x}} s^{*}_{\mathrm{vv}}(m) s'_{\mathrm{hh}}(m) + F_{\mathrm{tv}}^{\mathrm{co}*} F_{\mathrm{rv}}^{\mathrm{co}*} F_{\mathrm{tv}}^{\mathrm{x}} F_{\mathrm{rv}}^{\mathrm{x}} s^{*}_{\mathrm{vv}}(m) s'_{\mathrm{hh}}(m)\}\\
&\quad + 2\mathrm{Re}\{[F_{\mathrm{tv}}^{\mathrm{co}*} F_{\mathrm{rv}}^{\mathrm{co}*} F_{\mathrm{th}}^{\mathrm{x}} F_{\mathrm{rv}}^{\mathrm{co}} |s_{\mathrm{vv}}(m)|^2 + F_{\mathrm{tv}}^{\mathrm{co}*} F_{\mathrm{rv}}^{\mathrm{co}*} F_{\mathrm{th}}^{\mathrm{co}} F_{\mathrm{rv}}^{\mathrm{x}} s^{*}_{\mathrm{vv}}(m) s'_{\mathrm{hh}}(m)] e^{-j[\beta+\alpha_{\mathrm{v}}(m)-\alpha_{\mathrm{h}}(m)]}\}. \qquad \text{(A2)}
\end{aligned}
$$

Note that all higher-order products in which cross-polar pattern terms (i.e., $F_{ql}^{\mathrm{x}}$, where $q$ is t or r and $l$ is h or v), in $d\hat{S}_{\mathrm{h}}^{\mathrm{x}}(\Omega, m)$ or $d\hat{S}_{\mathrm{v}}^{\mathrm{x}}(\Omega, m)$, appear more than two times are discarded for simplicity, since it is assumed that they do not add appreciably to the sum. The terms

$$
\begin{aligned}
&\underbrace{\int_{\Omega_1} dV_{\mathrm{h}}(\mathbf{r},m)\,d\Omega_1 \int_{\Omega_2} dV_{\mathrm{h}}(\mathbf{r},m)\,d\Omega_2}_{d\Omega_1 \neq d\Omega_2}\\
&\underbrace{\int_{\Omega_1} dV_{\mathrm{v}}(\mathbf{r},m)\,d\Omega_1 \int_{\Omega_2} dV_{\mathrm{v}}(\mathbf{r},m)\,d\Omega_2}_{d\Omega_1 \neq d\Omega_2} \qquad \text{(A3)}
\end{aligned}
$$

are contributions from nonoverlapping $dV_6$. Because $s_{ll}(m)$ from different $dV_6$ volumes are uncorrelated, their ensemble averages are zero.

The total averaged power (over $M$ transmissions) from scatterers illuminated by radiation described by $F_{\mathrm{th}}^{\mathrm{co}}$, $F_{\mathrm{tv}}^{\mathrm{co}}$ whose returns are weighted by $F_{\mathrm{rh}}^{\mathrm{co}}$, $F_{\mathrm{rv}}^{\mathrm{co}}$ on reception is

$$
\begin{aligned}
\hat{S}_{\mathrm{h}}^{\mathrm{co}} &= \frac{1}{M}\sum_{m=0}^{M}\int_{\Omega} d\hat{S}_{\mathrm{h}}^{\mathrm{co}}(\Omega,m)\,d\Omega\\
\hat{S}_{\mathrm{v}}^{\mathrm{co}} &= \frac{1}{M}\sum_{m=0}^{M}\int_{\Omega} d\hat{S}_{\mathrm{hv}}^{\mathrm{co}}(\Omega,m)\,d\Omega. \qquad \text{(A4)}
\end{aligned}
$$

The total averaged power (over $M$ transmissions) from scatterers illuminated by both copolar and cross-polar radiation whose returns are weighted by the copolar and cross-polar patterns on reception are

$$
\begin{aligned}
\hat{S}_{\mathrm{h}}^{\mathrm{x}} &\approx \frac{1}{M}\sum_{m=0}^{M}\int_{\Omega} d\hat{S}_{\mathrm{h}}^{\mathrm{x}}(\Omega,m)\,d\Omega\\
\hat{S}_{\mathrm{v}}^{\mathrm{x}} &\approx \frac{1}{M}\sum_{m=0}^{M}\int_{\Omega} d\hat{S}_{\mathrm{v}}^{\mathrm{x}}(\Omega,m)\,d\Omega. \qquad \text{(A5)}
\end{aligned}
$$

Hence,

$$\langle \hat{S}_{\rm h}\rangle \approx \frac{1}{M}\sum_{m=0}^{M}\int_{\Omega}\langle d\hat{S}_{\rm h}(\Omega,m)\rangle\, d\Omega = \frac{1}{M}\sum_{m=0}^{M}\int_{\Omega}[\langle d\hat{S}_{\rm h}^{\rm co}(\Omega,m)\rangle + \langle d\hat{S}_{\rm h}^{\rm x}(\Omega,m)\rangle]\, d\Omega$$
$$\langle \hat{S}_{\rm v}\rangle \approx \frac{1}{M}\sum_{m=0}^{M}\int_{\Omega}\langle d\hat{S}_{\rm v}(\Omega,m)\rangle\, d\Omega = \frac{1}{M}\sum_{m=0}^{M}\int_{\Omega}[\langle d\hat{S}_{\rm h}^{\rm co}(\Omega,m)\rangle + \langle d\hat{S}_{\rm h}^{\rm x}(\Omega,m)\rangle]\, d\Omega, \tag{A6}$$

where

$$\begin{aligned}
\langle d\hat{S}_{\rm h}^{\rm co}(\Omega,m)\rangle &= S_{\rm h}|F_{\rm th}^{\rm co}F_{\rm rh}^{\rm co}|^2\int_{\Omega}d\Omega,\\
\langle d\hat{S}_{\rm h}^{\rm x}(\Omega,m)\rangle &= S_{\rm h}\Big[|F_{\rm tv}^{\rm x}|^2|F_{\rm rh}^{\rm co}|^2 + |F_{\rm tv}^{\rm co}|^2|F_{\rm rh}^{\rm x}|^2Z_{\rm dr}^{-1} + 2{\rm Re}\{F_{\rm th}^{\rm co*}F_{\rm rh}^{\rm co*}F_{\rm tv}^{\rm x}F_{\rm rh}^{\rm co}e^{j[\beta+\alpha_{\rm v}(m)-\alpha_{\rm h}(m)]}\}\\
&\quad + 2\frac{|\rho_{\rm hv}(0)|}{\sqrt{Z_{\rm dr}}}{\rm Re}\{(F_{\rm tv}^{\rm x*}F_{\rm rh}^{\rm co*}F_{\rm tv}^{\rm co}F_{\rm rh}^{\rm x} + F_{\rm th}^{\rm co*}F_{\rm rh}^{\rm co*}F_{\rm th}^{\rm x}F_{\rm rh}^{\rm x} + F_{\rm th}^{\rm co*}F_{\rm rh}^{\rm co*}F_{\rm tv}^{\rm co}F_{\rm rh}^{\rm x}e^{j[\beta+\alpha_{\rm v}(m)-\alpha_{\rm h}(m)]})e^{j\phi_{\rm DP}}\}\Big].\\
\langle d\hat{S}_{\rm v}^{\rm co}(\Omega,m)\rangle &= S_{\rm v}|F_{\rm tv}^{\rm co}F_{\rm rv}^{\rm co}|^2,\\
\langle d\hat{S}_{\rm v}^{\rm x}(\Omega,m)\rangle &= S_{\rm v}[|F_{\rm th}^{\rm x}|^2|F_{\rm rv}^{\rm co}|^2 + |F_{\rm th}^{\rm co}|^2|F_{\rm rv}^{\rm x}|^2Z_{\rm dr} + 2{\rm Re}\{F_{\rm tv}^{\rm co*}F_{\rm rv}^{\rm co*}F_{\rm th}^{\rm x}F_{\rm rv}^{\rm co}e^{-j[\beta+\alpha_{\rm v}(m)-\alpha_{\rm h}(m)]}\}\\
&\quad + 2|\rho_{\rm hv}(0)|\sqrt{Z_{\rm dr}}\,{\rm Re}\{(F_{\rm th}^{\rm x*}F_{\rm rv}^{\rm co*}F_{\rm th}^{\rm co}F_{\rm rv}^{\rm x} + F_{\rm tv}^{\rm co*}F_{\rm rv}^{\rm co*}F_{\rm tv}^{\rm x}F_{\rm rv}^{\rm x} + F_{\rm tv}^{\rm co*}F_{\rm rv}^{\rm co*}F_{\rm th}^{\rm co}F_{\rm rv}^{\rm x}e^{-j[\beta+\alpha_{\rm v}(m)-\alpha_{\rm h}(m)]})e^{-j\phi_{\rm DP}}\}].
\end{aligned} \tag{A7}$$

Note that in (A7) the uniform beamfilling is assumed. Consequently, the $S_{\rm h}, S_{\rm v}, Z_{\rm dr} = S_{\rm h}/S_{\rm v}, |\rho_{\rm hv}(0)|,$ and $\phi_{\rm DP}$ are independent of $\Omega$.

Using (16), an ensemble average of $\hat{Z}_{\rm DR}$ is

$$\langle \hat{Z}_{\rm DR}\rangle \approx 10\left\langle \log_{10}\left(\frac{\int_{\Omega}d\hat{S}_{\rm h}^{\rm co}(\Omega,m)\,d\Omega}{\int_{\Omega}d\hat{S}_{\rm v}^{\rm co}(\Omega,m)\,d\Omega}\right)\right\rangle + \frac{10}{\ln(10)}\frac{1}{M}\sum_{m=0}^{M-1}\left(\frac{\int_{\Omega}\langle d\hat{S}_{\rm h}^{\rm x}(\Omega,m)\rangle\,d\Omega}{\int_{\Omega}\langle d\hat{S}_{\rm h}^{\rm co}(\Omega,m)\rangle\,d\Omega} - \frac{\int_{\Omega}\langle d\hat{S}_{\rm v}^{\rm x}(\Omega,m)\rangle\,d\Omega}{\int_{\Omega}\langle d\hat{S}_{\rm v}^{\rm co}(\Omega,m)\rangle\,d\Omega}\right), \tag{A8}$$

which yields

$$\begin{aligned}
\langle \hat{Z}_{\rm DR}\rangle &\approx Z_{\rm DR} + 10\log_{10}\left(\frac{\int_{\Omega}|F_{\rm th}^{\rm co}F_{\rm rh}^{\rm co}|^2\,d\Omega}{\int_{\Omega}|F_{\rm tv}^{\rm co}F_{\rm rv}^{\rm co}|^2\,d\Omega}\right)\\
&\quad + \frac{10}{\ln(10)}\frac{1}{M}\sum_{m=0}^{M-1}\left(\frac{\int_{\Omega}[|F_{\rm tv}^{\rm x}|^2|F_{\rm rh}^{\rm co}|^2 + |F_{\rm tv}^{\rm co}|^2|F_{\rm rh}^{\rm x}|^2Z_{\rm dr}^{-1}]\,d\Omega}{\int_{\Omega}|F_{\rm th}^{\rm co}F_{\rm rh}^{\rm co}|^2\,d\Omega} - \frac{\int_{\Omega}[|F_{\rm th}^{\rm x}|^2|F_{\rm rv}^{\rm co}|^2 + |F_{\rm th}^{\rm co}|^2|F_{\rm rv}^{\rm x}|^2Z_{\rm dr}]\,d\Omega}{\int_{\Omega}|F_{\rm tv}^{\rm co}F_{\rm rv}^{\rm co}|^2\,d\Omega}\right.\\
&\quad + 2\frac{|\rho_{\rm hv}(0)|}{\sqrt{Z_{\rm dr}}}\frac{\int_{\Omega}{\rm Re}\{(F_{\rm tv}^{\rm x*}F_{\rm rh}^{\rm co*}F_{\rm tv}^{\rm co}F_{\rm rh}^{\rm x} + F_{\rm th}^{\rm co*}F_{\rm rh}^{\rm co*}F_{\rm th}^{\rm x}F_{\rm rh}^{\rm x} + F_{\rm th}^{\rm co*}F_{\rm rh}^{\rm co*}F_{\rm tv}^{\rm co}F_{\rm rh}^{\rm x}e^{j[\beta+\alpha_{\rm v}(m)-\alpha_{\rm h}(m)]})e^{j\phi_{\rm DP}}\}\,d\Omega}{\int_{\Omega}|F_{\rm th}^{\rm co}F_{\rm rh}^{\rm co}|^2\,d\Omega}\\
&\quad - 2|\rho_{\rm hv}(0)|\sqrt{Z_{\rm dr}}\,\frac{\int_{\Omega}{\rm Re}\{(F_{\rm th}^{\rm x*}F_{\rm rv}^{\rm co*}F_{\rm th}^{\rm co}F_{\rm rv}^{\rm x} + F_{\rm tv}^{\rm co*}F_{\rm rv}^{\rm co*}F_{\rm tv}^{\rm x}F_{\rm rv}^{\rm x} + F_{\rm tv}^{\rm co*}F_{\rm rv}^{\rm co*}F_{\rm th}^{\rm co}F_{\rm rv}^{\rm x}e^{-j[\beta+\alpha_{\rm v}(m)-\alpha_{\rm h}(m)]})e^{-j\phi_{\rm DP}}\}\,d\Omega}{\int_{\Omega}|F_{\rm tv}^{\rm co}F_{\rm rv}^{\rm co}|^2\,d\Omega}\\
&\quad \left. + 2\frac{\int_{\Omega}{\rm Re}\{F_{\rm th}^{\rm co*}F_{\rm rh}^{\rm co*}F_{\rm tv}^{\rm x}F_{\rm rh}^{\rm co}e^{j[\beta+\alpha_{\rm v}(m)-\alpha_{\rm h}(m)]}\}\,d\Omega}{\int_{\Omega}|F_{\rm th}^{\rm co}F_{\rm rh}^{\rm co}|^2\,d\Omega} - 2\frac{\int_{\Omega}{\rm Re}\{F_{\rm tv}^{\rm co*}F_{\rm rv}^{\rm co*}F_{\rm th}^{\rm x}F_{\rm rv}^{\rm co}e^{-j[\beta+\alpha_{\rm v}(m)-\alpha_{\rm h}(m)]}\}\,d\Omega}{\int_{\Omega}|F_{\rm tv}^{\rm co}F_{\rm rv}^{\rm co}|^2\,d\Omega}\right).
\end{aligned} \tag{A9}$$

The expansion in Taylor series can be avoided by computing $\langle \hat{Z}_{\rm DR} \rangle$ directly as

$$\langle \hat{Z}_{\rm DR} \rangle \approx 10 \log_{10} \left( \frac{\frac{1}{M} \sum_{m=0}^{M-1} \int_{\Omega} \langle d\hat{S}_{\rm h}(\Omega, m) \rangle \, d\Omega}{\frac{1}{M} \sum_{m=0}^{M-1} \int_{\Omega} \langle d\hat{S}_{\rm v}(\Omega, m) \rangle \, d\Omega} \right). \tag{A10}$$

Further, the cross correlation is

$$\begin{aligned} V_{\rm h}^*(\mathbf{r}, m) V_{\rm v}(\mathbf{r}, m) &= \int_{\Omega} dV_{\rm h}^*(\mathbf{r}, m) \, dV_{\rm v}(\mathbf{r}, m) \, d\Omega + \underbrace{\int_{\Omega_1} dV_{\rm h}(\mathbf{r}, m) \, d\Omega_1 \int_{\Omega_2} dV_{\rm v}(\mathbf{r}, m) \, d\Omega_2}_{d\Omega_1 \neq d\Omega_2} \\ &\approx \int_{\Omega} \{ [F_{\rm th}^{\rm co*} F_{\rm rh}^{\rm co*} F_{\rm tv}^{\rm co} F_{\rm rv}^{\rm co} e^{j\beta} + F_{\rm tv}^{\rm x*} F_{\rm rh}^{\rm co*} F_{\rm th}^{\rm x} F_{\rm rv}^{\rm co} e^{-j\beta} e^{j2[\alpha_{\rm h}(m) - \alpha_{\rm v}(m)]} + F_{\rm tv}^{\rm x*} F_{\rm rh}^{\rm co*} F_{\rm tv}^{\rm co} F_{\rm rv}^{\rm co} e^{j[\alpha_{\rm h}(m) - \alpha_{\rm v}(m)]} \\ &\quad + F_{\rm th}^{\rm co*} F_{\rm rh}^{\rm co*} F_{\rm th}^{\rm x} F_{\rm rv}^{\rm co} e^{j[\alpha_{\rm h}(m) - \alpha_{\rm v}(m)]}] s_{\rm hh}'^*(m) s_{\rm vv}(m) + [F_{\rm th}^{\rm co*} F_{\rm rh}^{\rm co*} F_{\rm tv}^{\rm x} F_{\rm rv}^{\rm x} e^{j\beta} + F_{\rm th}^{\rm co*} F_{\rm rh}^{\rm co*} F_{\rm th}^{\rm co} F_{\rm rv}^{\rm x} e^{j[\alpha_{\rm h}(m) - \alpha_{\rm v}(m)]} \\ &\quad + F_{\rm tv}^{\rm x*} F_{\rm rh}^{\rm co*} F_{\rm th}^{\rm co} F_{\rm rv}^{\rm x} e^{-j\beta} e^{j2[\alpha_{\rm h}(m) - \alpha_{\rm v}(m)]}] |s_{\rm hh}'(m)|^2 + [F_{\rm th}^{\rm x*} F_{\rm rh}^{\rm x*} F_{\rm tv}^{\rm co} F_{\rm rv}^{\rm co} e^{j\beta} + F_{\rm tv}^{\rm co*} F_{\rm rh}^{\rm x*} F_{\rm tv}^{\rm co} F_{\rm rv}^{\rm co} e^{j[\alpha_{\rm h}(m) - \alpha_{\rm v}(m)]} \\ &\quad + F_{\rm tv}^{\rm co*} F_{\rm rh}^{\rm x*} F_{\rm th}^{\rm x} F_{\rm rv}^{\rm co} e^{-j\beta} e^{j2[\alpha_{\rm h}(m) - \alpha_{\rm v}(m)]}] |s_{\rm vv}(m)|^2 + F_{\rm tv}^{\rm co*} F_{\rm rh}^{\rm x*} F_{\rm th}^{\rm co} F_{\rm rv}^{\rm x} s_{\rm vv}^*(m) s_{\rm hh}'(m) e^{-j\beta} e^{j2[\alpha_{\rm h}(m) - \alpha_{\rm v}(m)]} \} \, d\Omega \\ &\quad + \underbrace{\int_{\Omega_1} dV_{\rm h}(\mathbf{r}, m) \, d\Omega_1 \int_{\Omega_2} dV_{\rm v}(\mathbf{r}, m) \, d\Omega_2}_{d\Omega_1 \neq d\Omega_2}. \end{aligned} \tag{A11}$$

Hence,

$$\begin{aligned} \langle \hat{R}_{\rm hv}(0) \rangle &= \frac{1}{M} \sum_{m=0}^{M-1} \langle V_{\rm h}^*(\mathbf{r}, m) V_{\rm v}(\mathbf{r}, m) \rangle \\ &= \frac{1}{M} \sum_{m=0}^{M-1} \int_{\Omega} \langle dV_{\rm h}^*(\mathbf{r}, m) dV_{\rm v}(\mathbf{r}, m) \rangle \, d\Omega = \frac{1}{M} \sum_{m=0}^{M-1} \int_{\Omega} \langle d\hat{R}_{\rm hv}(\Omega, m, 0) \rangle \, d\Omega \\ &\approx \frac{1}{M} \sum_{m=0}^{M-1} \int_{\Omega} \{ \sqrt{S_{\rm h} S_{\rm v}} |\rho_{\rm hv}(0)| e^{j\phi_{\rm DP}} [F_{\rm th}^{\rm co*} F_{\rm rh}^{\rm co*} F_{\rm tv}^{\rm co} F_{\rm rv}^{\rm co} e^{j\beta} + F_{\rm tv}^{\rm x*} F_{\rm rh}^{\rm co*} F_{\rm tv}^{\rm co} F_{\rm rv}^{\rm co} e^{j[\alpha_{\rm h}(m) - \alpha_{\rm v}(m)]} \\ &\quad + F_{\rm tv}^{\rm x*} F_{\rm rh}^{\rm co*} F_{\rm th}^{\rm x} F_{\rm rv}^{\rm co} e^{-j\beta} e^{j2[\alpha_{\rm h}(m) - \alpha_{\rm v}(m)]} + F_{\rm th}^{\rm co*} F_{\rm rh}^{\rm co*} F_{\rm th}^{\rm x} F_{\rm rv}^{\rm co} e^{j[\alpha_{\rm h}(m) - \alpha_{\rm v}(m)]}] \\ &\quad + S_{\rm h} [ F_{\rm th}^{\rm co*} F_{\rm rh}^{\rm co*} F_{\rm tv}^{\rm x} F_{\rm rv}^{\rm x} e^{j\beta} + F_{\rm th}^{\rm co*} F_{\rm rh}^{\rm co*} F_{\rm th}^{\rm co} F_{\rm rv}^{\rm x} e^{j[\alpha_{\rm h}(m) - \alpha_{\rm v}(m)]} + F_{\rm tv}^{\rm x*} F_{\rm rh}^{\rm co*} F_{\rm th}^{\rm co} F_{\rm rv}^{\rm x} e^{-j\beta} e^{j2[\alpha_{\rm h}(m) - \alpha_{\rm v}(m)]} ] \\ &\quad + S_{\rm v} [ F_{\rm th}^{\rm x*} F_{\rm rh}^{\rm x*} F_{\rm tv}^{\rm co} F_{\rm rv}^{\rm co} e^{j\beta} + F_{\rm tv}^{\rm co*} F_{\rm rh}^{\rm x*} F_{\rm tv}^{\rm co} F_{\rm rv}^{\rm co} e^{j[\alpha_{\rm h}(m) - \alpha_{\rm v}(m)]} + F_{\rm tv}^{\rm co*} F_{\rm rh}^{\rm x*} F_{\rm th}^{\rm x} F_{\rm rv}^{\rm co} e^{-j\beta} e^{j2[\alpha_{\rm h}(m) - \alpha_{\rm v}(m)]} ] \\ &\quad + \sqrt{S_{\rm h} S_{\rm v}} |\rho_{\rm hv}(0)| e^{-j\phi_{\rm DP}} e^{-j\beta} F_{\rm th}^{\rm x*} F_{\rm rv}^{\rm co*} F_{\rm th}^{\rm co} F_{\rm rv}^{\rm x} e^{j2[\alpha_{\rm h}(m) - \alpha_{\rm v}(m)]} \} \, d\Omega, \end{aligned} \tag{A12}$$

and

$$\langle \hat{\phi}_{\rm DP} \rangle = \arg \left[ \frac{1}{M} \sum_{m=0}^{M-1} \int_{\Omega} \langle d\hat{R}_{\rm hv}(\Omega, m, 0) \rangle \, d\Omega \right]. \tag{A13}$$

An analytical expression for $\langle|\hat{\rho}_{hv}(0)|\rangle$ is [(15) in Galletti and Zrnić 2011]

$$\langle|\hat{\rho}_{hv}(0)|\rangle \approx \frac{\frac{1}{M}\sum_{m=0}^{M-1}\int_{\Omega}|\langle d\hat{R}_{hv}(\Omega,m,0)\rangle|\,d\Omega}{\sqrt{\left[\frac{1}{M}\sum_{m=0}^{M-1}\int_{\Omega}\langle d\hat{S}_{h}(\Omega,m)\rangle\,d\Omega\right]\left[\frac{1}{M}\sum_{m=0}^{M-1}\int_{\Omega}\langle d\hat{S}_{v}(\Omega,m)\rangle\,d\Omega\right]}}. \tag{A14}$$

Given the discrete antenna patterns, (A9) can be arranged by replacing the dependency on $\Omega$ with $n_\theta$, $m_\phi$ as

$$\begin{aligned}
\langle\hat{Z}_{DR}\rangle \approx Z_{DR} + 10\log_{10}&\left(\frac{\sum_{n_\theta=0}^{N_\theta-1}\sum_{m_\phi=0}^{M_\phi-1}|F_{th}^{co}F_{rh}^{co}|^2\sin[\Theta(n_\theta,m_\phi)]\Delta\theta\Delta\phi}{\sum_{n_\theta=0}^{N_\theta-1}\sum_{m_\phi=0}^{M_\phi-1}|F_{tv}^{co}F_{rv}^{co}|^2\sin[\Theta(n_\theta,m_\phi)]\Delta\theta\Delta\phi}\right)\\
&+\frac{10}{\ln(10)}\frac{1}{M}\sum_{m=0}^{M-1}\left(\frac{\sum_{n_\theta=0}^{N_\theta-1}\sum_{m_\phi=0}^{M_\phi-1}[|F_{rh}^{co}|^2|F_{tv}^{x}|^2+|F_{tv}^{co}|^2|F_{rh}^{x}|^2Z_{dr}^{-1}]\sin[\Theta(n_\theta,m_\phi)]\Delta\theta\Delta\phi}{\sum_{n_\theta=0}^{N_\theta-1}\sum_{m_\phi=0}^{M_\phi-1}|F_{th}^{co}F_{rh}^{co}|^2\sin[\Theta(n_\theta,m_\phi)]\Delta\theta\Delta\phi}\right.\\
&-\frac{\sum_{n_\theta=0}^{N_\theta-1}\sum_{m_\phi=0}^{M_\phi-1}[|F_{th}^{x}|^2|F_{rv}^{co}|^2+|F_{th}^{co}|^2|F_{rv}^{x}|^2Z_{dr}]\sin[\Theta(n_\theta,m_\phi)]\Delta\theta\Delta\phi}{\sum_{n_\theta=0}^{N_\theta-1}\sum_{m_\phi=0}^{M_\phi-1}|F_{tv}^{co}F_{rv}^{co}|^2\sin[\Theta(n_\theta,m_\phi)]\Delta\theta\Delta\phi}\\
&+2\frac{|\rho_{hv}(0)|}{Z_{dr}}\frac{\sum_{n_\theta=0}^{N_\theta-1}\sum_{m_\phi=0}^{M_\phi-1}\mathrm{Re}\{[F_{tv}^{x*}F_{rh}^{co*}F_{tv}^{co}F_{rh}^{x}+F_{th}^{co*}F_{rh}^{co*}F_{th}^{x}F_{rh}^{x}+F_{th}^{co*}F_{rh}^{co*}F_{tv}^{co}F_{rh}^{x}e^{j[\beta+\alpha_v(m)-\alpha_h(m)]}]e^{j\phi_{DP}}\}\sin[\Theta(n_\theta,m_\phi)]\Delta\theta\Delta\phi}{\sum_{n_\theta=0}^{N_\theta-1}\sum_{m_\phi=0}^{M_\phi-1}|F_{th}^{co}F_{rh}^{co}|^2\sin[\Theta(n_\theta,m_\phi)]\Delta\theta\Delta\phi}\\
&-2|\rho_{hv}(0)|Z_{dr}\frac{\sum_{n_\theta=0}^{N_\theta-1}\sum_{m_\phi=0}^{M_\phi-1}\mathrm{Re}\{[F_{th}^{x*}F_{rv}^{co*}F_{th}^{co}F_{rv}^{x}+F_{tv}^{co*}F_{rv}^{co*}F_{tv}^{x}F_{rv}^{x}+F_{tv}^{co*}F_{rv}^{co*}F_{th}^{co}F_{rv}^{x}e^{-j[\beta+\alpha_v(m)-\alpha_h(m)]}]e^{-j\phi_{DP}}\}\sin[\Theta(n_\theta,m_\phi)]\Delta\theta\Delta\phi}{\sum_{n_\theta=0}^{N_\theta-1}\sum_{m_\phi=0}^{M_\phi-1}|F_{tv}^{co}F_{rv}^{co}|^2\sin[\Theta(n_\theta,m_\phi)]\Delta\theta\Delta\phi}\\
&+2\frac{\sum_{n_\theta=0}^{N_\theta-1}\sum_{m_\phi=0}^{M_\phi-1}\mathrm{Re}\{F_{th}^{co*}F_{rh}^{co*}F_{tv}^{x}F_{rh}^{co}e^{j[\beta+\alpha_v(m)-\alpha_h(m)]}\}\sin[\Theta(n_\theta,m_\phi)]\Delta\theta\Delta\phi}{\sum_{n_\theta=0}^{N_\theta-1}\sum_{m_\phi=0}^{M_\phi-1}|F_{th}^{co}F_{rh}^{co}|^2\sin[\Theta(n_\theta,m_\phi)]\Delta\theta\Delta\phi}\\
&\left.-2\frac{\sum_{n_\theta=0}^{N_\theta-1}\sum_{m_\phi=0}^{M_\phi-1}\mathrm{Re}\{F_{tv}^{co*}F_{rv}^{co*}F_{th}^{x}F_{rv}^{co}e^{-j[\beta+\alpha_v(m)-\alpha_h(m)]}\}\sin[\Theta(n_\theta,m_\phi)]\Delta\theta\Delta\phi}{\sum_{n_\theta=0}^{N_\theta-1}\sum_{m_\phi=0}^{M_\phi-1}|F_{tv}^{co}F_{rv}^{co}|^2\sin[\Theta(n_\theta,m_\phi)]\Delta\theta\Delta\phi}\right),
\end{aligned} \tag{A15}$$

where it is understood that all antenna patterns are functions of $n_\theta$, $m_\phi$. In the case of (A10), (A13), and (A14),

$$\langle \hat{Z}_{\mathrm{DR}} \rangle \approx 10\log_{10}\left( \frac{\sum_{n_\theta=0}^{N_\theta-1}\sum_{m_\phi=0}^{M_\phi-1}\frac{1}{M}\sum_{m=0}^{M-1}\langle d\hat{S}_{\mathrm{h}}(n_\theta,m_\phi,m)\rangle \sin[\Theta(n_\theta,m_\phi)]\Delta\theta\Delta\phi}{\sum_{n_\theta=0}^{N_\theta-1}\sum_{m_\phi=0}^{M_\phi-1}\frac{1}{M}\sum_{m=0}^{M-1}\langle d\hat{S}_{\mathrm{v}}(n_\theta,m_\phi,m)\rangle \sin[\Theta(n_\theta,m_\phi)]\Delta\theta\Delta\phi} \right)$$

$$\langle \hat{\phi}_{\mathrm{DP}} \rangle = \arg\left[ \sum_{n_\theta=0}^{N_\theta-1}\sum_{m_\phi=0}^{M_\phi-1}\frac{1}{M}\sum_{m=0}^{M-1}\langle d\hat{R}_{\mathrm{hv}}(n_\theta,m_\phi,m,0)\rangle \sin[\Theta(n_\theta,m_\phi)]\Delta\theta\Delta\phi \right]$$

$$\langle |\hat{\rho}_{\mathrm{hv}}(0)| \rangle \approx \frac{\sum_{n_\theta=0}^{N_\theta-1}\sum_{m_\phi=0}^{M_\phi-1}\left|\frac{1}{M}\sum_{m=0}^{M-1}\langle d\hat{R}_{\mathrm{hv}}(n_\theta,m_\phi,m,0)\rangle\right| \sin[\Theta(n_\theta,m_\phi)]\Delta\theta\Delta\phi}{\sqrt{\sum_{n_\theta=0}^{N_\theta-1}\sum_{m_\phi=0}^{M_\phi-1}\frac{1}{M}\sum_{m=0}^{M-1}\langle d\hat{S}_{\mathrm{h}}(n_\theta,m_\phi,m)\rangle \sin[\Theta(n_\theta,m_\phi)]\Delta\theta\Delta\phi \times \sum_{n_\theta=0}^{N_\theta-1}\sum_{m_\phi=0}^{M_\phi-1}\frac{1}{M}\sum_{m=0}^{M-1}\langle d\hat{S}_{\mathrm{v}}(n_\theta,m_\phi,m)\rangle \sin[\Theta(n_\theta,m_\phi)]\Delta\theta\Delta\phi}} \tag{A16}$$

where full expressions are omitted for brevity. Then,

$$\begin{aligned} \mathrm{BIAS}\ \hat{Z}_{\mathrm{DR}} &= \langle \hat{Z}_{\mathrm{DR}} \rangle - Z_{\mathrm{DR}} \\ \mathrm{BIAS}\ |\hat{\rho}_{\mathrm{hv}}(0)| &= \langle |\hat{\rho}_{\mathrm{hv}}(0)| \rangle - |\rho_{\mathrm{hv}}(0)| \\ \mathrm{BIAS}\ \hat{\phi}_{\mathrm{DP}} &= \langle \hat{\phi}_{\mathrm{DP}} \rangle - \phi_{\mathrm{DP}}. \end{aligned} \tag{A17}$$

## APPENDIX B

### Derivation of Analytical Bias Expressions for the AHV Mode

In this appendix a derivation of analytical formulas for the mathematical expectations of $\hat{Z}_{\mathrm{DR}}$, $|\hat{\rho}_{\mathrm{hv}}(0)|$, and $\hat{\phi}_{\mathrm{DP}}$ in the AHV mode is presented. The derivation is used to produce the theoretical bias expressions. The formulas are derived by following the model, which uses $\mathbf{S}$, introduced in the text.

Following the same approach as in appendix A yields

$$\begin{aligned} \langle \hat{S}_{\mathrm{h}} \rangle &\approx \frac{2}{M}\sum_{m=0}^{M/2-1}\int_\Omega \langle d\hat{S}_{\mathrm{h}}(\Omega,2m)\rangle\, d\Omega \\ \langle \hat{S}_{\mathrm{v}} \rangle &\approx \frac{2}{M}\sum_{m=0}^{M/2-1}\int_\Omega \langle d\hat{S}_{\mathrm{v}}(\Omega,2m+1)\rangle\, d\Omega \\ \langle \hat{R}_a \rangle &\approx \int_\Omega \langle d\hat{R}_a(\Omega)\rangle\, d\Omega \frac{2}{M}\sum_{m=0}^{M/2-1} V_{\mathrm{h}}^*(2m)V_{\mathrm{v}}(2m+1) \\ \langle \hat{R}_b \rangle &\approx \int_\Omega \langle d\hat{R}_b(\Omega)\rangle\, d\Omega \\ \langle \hat{R}_{\mathrm{h}}(2) \rangle &\approx \int_\Omega \langle d\hat{R}_{\mathrm{h}}(\Omega,2)\rangle\, d\Omega \\ \langle \hat{R}_{\mathrm{v}}(2) \rangle &\approx \int_\Omega \langle d\hat{R}_{\mathrm{v}}(\Omega,2)\rangle\, d\Omega, \end{aligned} \tag{B1}$$

where

$$\langle d\hat{S}_{\rm h}(\Omega,2m)\rangle \approx S_{\rm h}\left[|F_{\rm th}^{\rm co}F_{\rm rh}^{\rm co}|^2+|F_{\rm th}^{\rm x}F_{\rm rh}^{\rm x}|^2\frac{1}{Z_{\rm dr}}+2{\rm Re}\{(F_{\rm th}^{\rm co}F_{\rm rh}^{\rm co})^*F_{\rm th}^{\rm x}F_{\rm rh}^{\rm x}e^{j\phi_{\rm DP}}\}\frac{|\rho_{\rm hv}(0)|}{\sqrt{Z_{\rm dr}}}\right]$$

$$\langle d\hat{S}_{\rm v}(\Omega,2m+1)\rangle \approx S_{\rm v}\left[|F_{\rm tv}^{\rm co}F_{\rm rv}^{\rm co}|^2+|F_{\rm tv}^{\rm x}F_{\rm rv}^{\rm x}|^2Z_{\rm dr}+2{\rm Re}\{(F_{\rm tv}^{\rm co}F_{\rm rv}^{\rm co})^*F_{\rm tv}^{\rm x}F_{\rm rv}^{\rm x}e^{-j\phi_{\rm DP}}\}|\rho_{\rm hv}(0)|\sqrt{Z_{\rm dr}}\right]$$

$$\langle d\hat{R}_a(\Omega)\rangle \approx \sqrt{\hat{S}_{\rm h}\hat{S}_{\rm v}}\left[(F_{\rm th}^{\rm co}F_{\rm rh}^{\rm co})^*F_{\rm tv}^{\rm co}F_{\rm rv}^{\rm co}|\rho_{\rm hv}(0)|e^{j\phi_{\rm DP}}+\frac{(F_{\rm th}^{\rm co}F_{\rm rh}^{\rm co})^*F_{\rm tv}^{\rm x}F_{\rm rv}^{\rm x}}{\sqrt{Z_{\rm dr}}}+(F_{\rm th}^{\rm x}F_{\rm rh}^{\rm x})^*F_{\rm tv}^{\rm co}F_{\rm rv}^{\rm co}\sqrt{Z_{\rm dr}}\right.$$
$$\left.+(F_{\rm th}^{\rm x}F_{\rm rh}^{\rm x})^*F_{\rm tv}^{\rm x}F_{\rm rv}^{\rm x}|\rho_{\rm hv}(0)|e^{-j\phi_{\rm DP}}\right]\rho(1)e^{j\beta}$$

$$\langle d\hat{R}_b(\Omega)\rangle \approx \sqrt{\hat{S}_{\rm h}\hat{S}_{\rm v}}\left[F_{\rm th}^{\rm co}F_{\rm rh}^{\rm co}(F_{\rm tv}^{\rm co}F_{\rm rv}^{\rm co})^*|\rho_{\rm hv}(0)|e^{-j\phi_{\rm DP}}+\frac{F_{\rm th}^{\rm x}F_{\rm rh}^{\rm x}(F_{\rm tv}^{\rm co}F_{\rm rv}^{\rm co})^*}{\sqrt{Z_{\rm dr}}}F_{\rm th}^{\rm co}F_{\rm rh}^{\rm co}(F_{\rm tv}^{\rm x}F_{\rm rv}^{\rm x})^*\sqrt{Z_{\rm dr}}\right.$$
$$\left.+F_{\rm th}^{\rm x}F_{\rm rh}^{\rm x}(F_{\rm tv}^{\rm x}F_{\rm rv}^{\rm x})^*|\rho_{\rm hv}(0)|e^{j\phi_{\rm DP}}\right]\rho(1)e^{-j\beta}$$

$$\langle d\hat{R}_{\rm h}(\Omega,2)\rangle \approx \hat{S}_{\rm h}\left[|F_{\rm th}^{\rm co}F_{\rm rh}^{\rm co}|^2+\frac{|\rho_{\rm hv}(0)|}{\sqrt{Z_{\rm dr}}}2{\rm Re}\{(F_{\rm th}^{\rm co}F_{\rm rh}^{\rm co})^*F_{\rm th}^{\rm x}F_{\rm rh}^{\rm x}e^{j\phi_{\rm DP}}\}+\frac{|F_{\rm th}^{\rm x}F_{\rm rh}^{\rm x}|^2}{Z_{\rm dr}}\right]\rho(2)$$

$$\langle d\hat{R}_{\rm v}(\Omega,2)\rangle \approx \hat{S}_{\rm v}\left[|F_{\rm tv}^{\rm co}F_{\rm rv}^{\rm co}|^2+|F_{\rm tv}^{\rm x}F_{\rm rv}^{\rm x}|^2Z_{\rm dr}+|\rho_{\rm hv}(0)|\sqrt{Z_{\rm dr}}2{\rm Re}\{(F_{\rm tv}^{\rm x}F_{\rm rv}^{\rm x})^*F_{\rm tv}^{\rm co}F_{\rm rv}^{\rm co}e^{j\phi_{\rm DP}}\}\right]\rho(2), \quad \text{(B2)}$$

and

$$\rho(n)=e^{-\{[(\pi\sigma_{\rm v}n\upsilon/\upsilon_a)^2/2]+[j\pi n(\upsilon/\upsilon_a)]\}}. \quad \text{(B3)}$$

In (B3), $\upsilon$ is the mean velocity (Doviak and Zrnić 1993). Also, note that in (B2) no higher-order terms are discarded. Using the expressions in (B1) and replacing integrals with sums across the antenna patterns (as in appendix A), the ensemble averages of polarimetric variable estimates are computed as

$$\langle\hat{Z}_{\rm DR}\rangle = 10\log_{10}\left(\frac{\langle\hat{S}_{\rm h}\rangle}{\langle\hat{S}_{\rm v}\rangle}\right)$$

$$|\hat{\rho}_{\rm hv}(0)| = \frac{|\langle\hat{R}_a\rangle|+|\langle\hat{R}_b\rangle|}{2(\langle\hat{S}_{\rm h}\rangle\langle\hat{S}_{\rm v}\rangle)^{3/8}|\langle\hat{R}_{\rm h}(2)\rangle\langle\hat{R}_{\rm v}(2)\rangle|^{1/8}}$$

$$\hat{\phi}_{\rm DP} = \frac{\arg[\langle\hat{R}_a\rangle\langle\hat{R}_b\rangle^*]}{2}. \quad \text{(B4)}$$

## REFERENCES


Balakrishnan, N., and D. S. Zrnić, 1990: Use of polarization to characterize precipitation and discriminate large hail. *J. Atmos. Sci.*, **47**, 1525–1540, doi:10.1175/1520-0469(1990)047<1525:UOPTCP>2.0.CO;2.

Balanis, C. A., 2005: *Antenna Theory*. John Wiley & Sons, 1047 pp.

Bringi, V. N., and V. Chandrasekar, 2001: *Polarimetric Doppler Weather Radar: Principles and Applications*. Cambridge University Press, 664 pp.

Chandrasekar, V., and R. J. Keeler. 1993: Antenna pattern analysis and measurements for multiparameter radars. *J. Atmos. Oceanic Technol.*, **10**, 674–683, doi:10.1175/1520-0426(1993)010<0674:APAAMF>2.0.CO;2.

Conway, D., J. Herd, M. Fosberry, M. Harger, C. Weigand, M. Yeary, and K. Hondl, 2013: On the development of a tileable LRU for the nextgen surveillance and weather radar capability program. *2013 IEEE International Symposium on Phased Array Systems and Technology*, IEEE, 490–493, doi:10.1109/ARRAY.2013.6731877.

Doviak, R. J., and D. S. Zrnić, 1993: *Doppler Radar and Weather Observations*. Academic Press, 562 pp.

——, V. Bringi, A. Ryzhkov, A. Zahrai, and D. Zrnić, 2000: Considerations for polarimetric upgrades to operational WSR-88D radars. *J. Atmos. Oceanic Technol.*, **17**, 257–278, doi:10.1175/1520-0426(2000)017<0257:CFPUTO>2.0.CO;2.

Galati, G., and G. Pavan, 1995: Computer simulation of weather radar signals. *Simul. Pract. Theory*, **3**, 17–44, doi:10.1016/0928-4869(95)00009-I.

Galletti, M., and D. S. Zrnić, 2011: Bias in copolar correlation coefficient caused by antenna radiation patterns. *IEEE Trans. Geosci. Remote Sens.*, **49**, 2274–2280, doi:10.1109/TGRS.2010.2095019.

Ivić, I. R., and A. Byrd, 2015: A first look at the MPAR dual-polarization phased-array-radar mobile demonstrator. *37th Conf. on Radar Meteorology*, Norman, OK, Amer. Meteor. Soc., 21. [Available online at https://ams.confex.com/ams/37RADAR/webprogram/Paper275179.html.]

——, and R. J. Doviak, 2016: Evaluation of phase coding to mitigate differential reflectivity bias in polarimetric PAR. *IEEE Trans. Geosci. Remote Sens.*, **54**, 431–451, doi:10.1109/TGRS.2015.2459047.

Lei, L., G. Zhang, R. J. Doviak, and S. Karimkashi, 2015: Comparison of theoretical biases in estimating polarimetric properties of precipitation with weather radar using parabolic

reflector, or planar and cylindrical arrays. *IEEE Trans. Geosci. Remote Sens.*, **53**, 4313–4327, doi:10.1109/TGRS.2015.2395714.

Ludwig, A., 1973: The definition of cross polarization. *IEEE Trans. Antennas Propag.*, **21**, 116–117, doi:10.1109/TAP.1973.1140406.

Mailloux, R. J., 2005: *Phased Array Antenna Handbook*. Artech House, 496 pp.

Melnikov, V. M., and D. S. Zrnić, 2015: On the alternate transmission mode for polarimetric phased array weather radar. *J. Atmos. Oceanic Technol.*, **32**, 220–233, doi:10.1175/JTECH-D-13-00176.1.

Oguchi, T., 1983: Electromagnetic wave propagation and scattering in rain and other hydrometeors. *Proc. IEEE*, **71**, 1029–1078, doi:10.1109/PROC.1983.12724.

Pointin, Y., D. Ramond, and J. Fournet-Fayard, 1988: Radar differential reflectivity $Z_{DR}$: A real-case evaluation of errors induced by antenna characteristics. *J. Atmos. Oceanic Technol.*, **5**, 416–423, doi:10.1175/1520-0426(1988)005<0416:RDRARC>2.0.CO;2.

Pozar, D. M., 1994: The active element pattern. *IEEE Trans. Antennas Propag.*, **42**, 1176–1178, doi:10.1109/8.310010.

Ryzhkov, A. V., and D. S. Zrnić, 2007: Depolarization in ice crystals and its effect on radar polarimetric measurements. *J. Atmos. Oceanic Technol.*, **24**, 1256–1267, doi:10.1175/JTECH2034.1.

——, ——, J. C. Hubbert, V. N. Bringi, J. Vivekanandan, and E. A. Brandes, 2002: Polarimetric radar observations and interpretation of co-cross-polar correlation coefficients. *J. Atmos. Oceanic Technol.*, **19**, 340–354, doi:10.1175/1520-0426-19.3.340.

Sachidananda, M., and D. S. Zrnić, 1985: $Z_{DR}$ measurement considerations for a fast scan capability radar. *Radio Sci.*, **20**, 907–922, doi:10.1029/RS020i004p00907.

Stapor, D. P., and T. Pratt, 1984: A generalized analysis of dual-polarization radar measurements in rain. *Radio Sci.*, **19**, 90–98, doi:10.1029/RS019i001p00090.

Wang, Y., and V. Chandrasekar, 2006: Polarization isolation requirements for linear dual-polarization weather radar in simultaneous transmission mode of operation. *IEEE Trans. Geosci. Remote Sens.*, **44**, 2019–2027, doi:10.1109/TGRS.2006.872138.

Weadon, M., P. Heinselman, D. Forsyth, W. E. Benner, G. S. Torok, and J. Kimpel, 2009: Multifunction phased array radar. *Bull. Amer. Meteor. Soc.*, **90**, 385–389, doi:10.1175/2008BAMS2666.1.

Zrnić, D. S., 1975: Simulation of weatherlike Doppler spectra and signals. *J. Appl. Meteor.*, **14**, 619–620, doi:10.1175/1520-0450(1975)014<0619:SOWDSA>2.0.CO;2.

——, and A. V. Ryzhkov, 1999: Polarimetry for weather surveillance radars. *Bull. Amer. Meteor. Soc.*, **80**, 389–406, doi:10.1175/1520-0477(1999)080<0389:PFWSR>2.0.CO;2.

——, ——, J. M. Straka, Y. Liu, and J. Vivekanandan, 2001: Testing a procedure for automatic classification of hydrometeor types. *J. Atmos. Oceanic Technol.*, **18**, 892–913, doi:10.1175/1520-0426(2001)018<0892:TAPFAC>2.0.CO;2.

——, and Coauthors, 2007: Agile beam phased array radar for weather observations. *Bull. Amer. Meteor. Soc.*, **88**, 1753–1766, doi:10.1175/BAMS-88-11-1753.

——, R. J. Doviak, G. Zhang, and R. V. Ryzhkov, 2010: Bias in differential reflectivity due to cross-coupling through the radiation patterns of polarimetric weather radars. *J. Atmos. Oceanic Technol.*, **27**, 1624–1637, doi:10.1175/2010JTECHA1350.1.

——, V. M. Melnikov, and R. J. Doviak, 2012: Issues and challenges for polarimetric measurement of weather with an agile beam phased array radar. NOAA/NSSL Rep., 119 pp. [Available online at http://www.nssl.noaa.gov/publications/mpar_reports/MPAR-WEB_RPT-1_071412-7_May_2_2013_wo_comments.pdf.]

——, R. J. Doviak, V. M. Melnikov, and I. R. Ivić, 2014: Signal design to suppress coupling in the polarimetric phased array radar. *J. Atmos. Oceanic Technol.*, **31**, 1063–1077, doi:10.1175/JTECH-D-13-00037.1.